TUDelft

Delft University of Technology

Lattice structures made by laser powder bed fusion

Mirzaali, Mohammad J.; Azarniya, Abolfazl; Sovizi, Saeed; Zhou, Jie; Zadpoor, Amir A.

Citation (APA)
Mirzaali, M. J., Azarniya, A., Sovizi, S., Zhou, J., & Zadpoor, A. A. (2021). Lattice structures made by laser powder bed fusion. In I. Yadroitsev, I. Yadroitsava, A. du Plessis, & E. MacDonald (Eds.), *Fundamentals of Laser Powder Bed Fusion of Metals: Additive Manufacturing Materials and Technologies* (pp. 423-465). Elsevier. https://doi.org/10.1016/B978-0-12-824090-8.00020-2

Important note
To cite this publication, please use the final published version (if applicable).
Please check the document version above.

Lattice structures made by laser powder bed fusion

16

Mohammad J. Mirzaali[1], Abolfazl Azarniya[2], Saeed Sovizi[3], Jie Zhou[1], Amir A. Zadpoor[1]

[1]Department of Biomechanical Engineering, Faculty of Mechanical, Maritime, and Materials Engineering, Delft University of Technology (TU Delft), Delft, the Netherlands; [2]Department of Mechanical Engineering, National University of Singapore, Singapore, Singapore; [3]Independent Researcher, Tehran, Iran

Chapter outline

16.1   Introduction

Foam-like porous structures have been widely used in the past to design load-bearing cellular materials (both open- and closed-cell). These foam-like materials have been traditionally fabricated using conventional manufacturing techniques, including liquid-state processes (e.g., direct forming, spray forming) and solid-state processes (e.g., powder metallurgy, sintering of powders and fibers), or through electro- or vapor-deposition (Ryan et al., 2006; Banhart, 2001; Mirzaali et al., 2016a, 2017c). Although the statistical distribution of the sizes and the shape of the pores can be adjusted to some extent by changing the processing parameters of conventional techniques, such fabrication techniques suffer from multiple inherent limitations, the most important of which is the lack of form-freedom. Additive manufacturing (AM) processes, on the other hand, offer the freedom to precisely control the sizes and architecture of pores at the microscale (Bose et al., 2013; Murr et al., 2010; Zadpoor, 2017). AM processes also provide the opportunity to design organic geometries with complex internal architectures and passages that are otherwise impossible to create or control by using conventional manufacturing techniques, such as casting or molding (Gokuldoss et al., 2017).

In this chapter, we are primarily concerned with metallic lattice structures. Powder bed fusion processes are perhaps the most widely used AM techniques for the fabrication of such structures. Even though the energy source may be either an electron beam or a laser beam, we will focus on the laser beam−based powder bed fusion (L-PBF) process. The L-PBF technique allows for creating porous structures made of metals, polymers, or ceramics with complex microarchitectures at high resolutions (Frazier, 2014; Mirzaali et al., 2019a).

Although the L-PBF technique is generally considered to offer form-freedom, there are still some design constraints that need to be taken into account. Several guidelines (Kranz et al., 2015) have been proposed in the past to deal with the limitations of the L-PBF process and to define the processibility windows. The relevant topics in this regard include the minimum feature size (e.g., wall thickness, edges, and corners),

the orientation of the lattice with respect to the build direction, the sizes of the over-hangs, and the requirements regarding the design of support structures and their removal (Wang et al., 2016). Overhangs are one of the most important aspects that need to be carefully considered, as they can create undesired defects in lattices (Su et al., 2012; Calignano, 2014). In this context, overhangs refer to the parts of lattice structures that are not self-supporting. As the manufacturing process progresses, there are no solidified sections from the previous layers that support overhangs, making them susceptible to defect formation. Successful fabrication of overhangs is, therefore, often dependent on the proper choice of the fabrication angle (Su et al., 2012). For overhangs exceeding a specific size and having a smaller angle with the power bed than a specific threshold, support structures need to be used. These support structures need to be removed during post-processing, which can damage the AM parts.

16.2 Geometrical design

The development of lattice structures starts with geometrical design. Lattice structures can be categorized as being either open-cell or closed-cell. Only open-cell lattices can be fabricated using AM techniques, as it is impossible to remove the entrapped powder particles in fully closed-cell lattices. Several principles have been proposed for the geometrical design of lattice structures, which we will briefly review hereafter.

16.2.1 Library-based designs

Traditional design strategies include computer-aided design (CAD), implicit surfaces, and image-based design (Giannitelli et al., 2014). CAD-based design can be obtained using open-source or commercial CAD software. The CAD design may be trans-formed into the standard tessellation language (STL) format to facilitate the manufacturing processes. In addition to STL files, a vector-based approach (Ahmadi et al., 2017) can also be implemented to create laser scanning lines for 3D printing. There are several advantages to the vector-based approach as compared to STL files, including the easier manipulation of the files due to a smaller size of the geometry file, which may facilitate the design of more complex structures (see Chapter 5 for more information).

The final lattice structure may have either a regular or an irregular microarchitec-ture. Regular lattices are usually made by repeating one or more types of unit cells in different spatial directions. Several types of unit cells have been proposed in the past, such as cubic or prismatic unit cells. The unit cells can be categorized into two main types, namely strut-based (beam-based) or sheet-based. In irregular or random lattices, no specific repeating unit cells can be found.

16.2.1.1 Strut-based unit cells

Most metallic lattices studied to date are the beam-based ones, where beam-like struc-tural elements (i.e., struts) are spatially arranged to create the basic unit cell

(Fig. 16.1a,b,e,f). The dimensions and spatial arrangement of the struts determine the geometry and topology (e.g., connectivity) of the repeating unit cell, the morphological parameters of the lattice structures (e.g., pore size, relative density), and the overall physical properties of the resulting porous materials (Maconachie et al., 2019). Some examples of strut-based unit cells are body centered cubic (BCC), face centered cubic (FCC) (Maskery et al., 2017; Zadpoor, 2019), cubic, diamond, and octet-truss (Yavari et al., 2015).
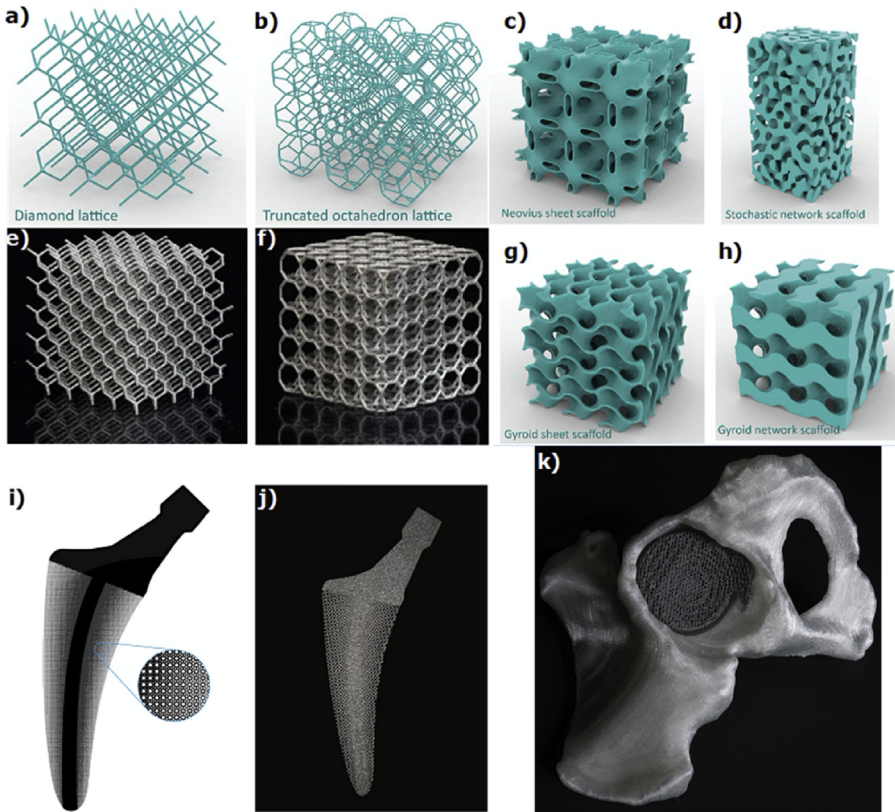
Figure 16.1 There are several strategies for the design of the microarchitectures of AM lattices. Examples include strut-based (a, b) and sheet-based (c, d, and g, h) CAD designs (Callens et al., 2020). These strut-based lattices can be fabricated by the L-PBF technique, for example, using Ti-alloys (e.g., Ti6Al4V (de Jonge et al., 2019) (e, f)). Another approach to the design of the microarchitecture of AM lattices is to apply optimization methods, which can result in functionally graded porous structures (i, j). The geometry of lattices can also be based on computed tomography (CT) images of spongy bone which allow for the fabrication of patient-specific implants (Zadpoor, 2017) (k).
(i, j) Reprinted from Garner et al., 2019. Copyright (2020), with permission from Elsevier.

From a mechanical viewpoint, lattice structures may be classified as being either bending-dominated or stretch-dominated. The elastic properties of stretch-dominated unit cells are higher than bending-dominated unit cells (Deshpande et al., 2001b). However, pure stretching or pure bending lattices can hardly be achieved, as there is usually a combination of bending and stretching in a unit cell. For a beam-based unit cell with s struts and n joints (i.e., strut intersections), the Maxwell number (i.e., $M = s - 3n + 6$) can be used to determine whether the unit cell is bending-dominated ($M < 0$) or stretch-dominated ($M \geq 0$) (Deshpande et al., 2001a).

16.2.1.2   Sheet-based unit cells

The structural elements constituting sheet-based unit cells are the surfaces (shells) that may be defined using mathematical equations. One class of sheet-based unit cells is the triply periodic minimal surfaces (TPMS) that offer a high level of flexibility in the design of lattice structures. In TPMS, pores are fully interconnected, making them suitable for tissue engineering applications (Kapfer et al., 2011; Yoo, 2011a,b; Bobbert et al., 2017). Another unique property of TPMS-based porous structures is that they exhibit a mean surface curvature of zero (Zadpoor, 2015; Bobbert et al., 2017). AM of high-quality TPMS geometries may be challenging due to the difficulties in achieving parts with high surface quality. Some examples of TPMS are primitive, I-WP, gyroid, Neovius, and diamond (Fig. 16.1c,g, and h).

16.2.1.3   Nonuniform designs

Both the type and dimensions of unit cells can be changed to create nonuniform lattice structures, such as those incorporating functional gradients. AM of porous structures with functional gradients has recently gained much attention (Choy et al., 2017; Loh et al., 2018), particularly for biomedical applications (Han et al., 2018; Monzón et al., 2018). Such graded designs can reduce stress concentrations and make it possible to satisfy contradictory design requirements. AM of functionally graded lattice structures is, however, challenging due to their geometrical complexity, particularly if stochastic or disordered design features are included.

Disordered lattice structures (Fig. 16.1d) may have some advantages over ordered lattices. First, random lattices offer a broader range of properties than the ordered ones, making it possible to change the properties more smoothly. For example, independent tuning of the elastic modulus and Poisson's ratio can be more easily achieved using random networks (Mirzaali et al., 2017b). Second, due to their inherently irregular design, random networks are less susceptible to local defects resulting from the AM process. Finally, the design of random networks is simpler than ordered networks, particularly when several types of unit cells (e.g., stretch-dominated and bending-dominated) need to be combined.

16.2.1.4 Isotropy/anisotropy

The theoretical upper and lower bounds (i.e., C_1 and C_2) of isotropic porous structure in 3D can be defined in terms of their elastic modulus (E) and Poisson's ratio (ν) as $0 < \dfrac{E(\nu)}{3(1 - 2\nu)} < C_1, 0 < \dfrac{E(\nu)}{2(1 + \nu)} < C_2$ (Hashin and Shtrikman, 1963), where,

$$C_1 = E_b \left(\frac{1}{3(1 - 2\nu_b)} + \frac{1 - \phi}{\dfrac{(1 - 2\nu_b)(1 + \nu_b)\phi}{(1 - \nu_b)} - 3(1 - 2\nu_b)} \right),$$

$$C_2 = E_b \left(\frac{1}{2(1 + \nu_b)} + \frac{1 - \phi}{\dfrac{4(4 - 5\nu_b)(1 + \nu_b)\phi}{15(1 - \nu_b)} - 2(1 + \nu_b)} \right)$$

E_b and ν_b are, respectively, the elastic modulus and Poisson's ratio of the base material, and ϕ is defined as the volume fraction of the lattice structure.

Anisotropic lattices may, however, be used to increase the load transfer efficiency of the lattice structures in specific directions. Such anisotropic lattices can exceed those limits in selected directions (Berger et al., 2017).

16.2.2 Topology optimization

Topology optimization can be used to computationally design optimal lattices. Several optimization approaches have been developed (Bendsoe and Sigmund, 2013), particularly using "inverse homogenization" techniques (Sánchez-Palencia, 1980; Bensoussan et al., 2011) that allow for finding a spatial arrangement of unit cells and material distribution, thereby giving rise to the desired (unusual) properties, such as a negative thermal expansion coefficient (Sigmund and Torquato, 1997).

Different objective functions can be used for the design of AM lattices. One such objective function is maximizing the specific stiffness (stiffness to mass ratio), which may result in lattices with trabecular bone-like microarchitectures (Garner et al., 2019; Wu et al., 2017a). There are optimization models based on bone tissue adaptation processes (Zadpoor et al., 2013; Zadpoor, 2013, 2017), which are useful for the design of bone substitutes (Fraldi et al., 2010; Chuah et al., 2010; Hollister et al., 2002) (Fig. 16.1i,j). Other objective functions, such as strain energy, can be used as well. Multi-physics topology optimization algorithms can optimize multiple objective functions simultaneously (Zhou et al., 2009), for example, to combine maximum bulk modulus or elastic modulus with specific values of permeability (Guest and Prévost, 2006; Ryan et al., 2006). There are several optimization techniques involved in finding the optimized topology of lattice structures with multifunctional properties, including evolutionary structural optimization (ESO) (Xie and Steven, 1993, 1997), solid isotropic material with penalization (SIMP) (Zhou and Rozvany, 1991; Bendsøe, 1989), bidirectional evolutionary structural optimization (BESO) (Huang et al., 2009;

Huang and Xie, 2007), and level-set algorithms (Wang et al. 2003). An increasing number of optimization tools (e.g., TOSCA, Pareto works, and PLATO (Blacker et al., 2015)) and freely available codes (Blacker et al., 2015) can be used for such design purposes. Integrating the specific requirements of AM processes into (topology) optimization algorithms is an active area of research (Challis et al., 2010; Xiao et al., 2013). An example of such integrations is the algorithms that deal with optimizing the arrangements of support materials during AM processes (e.g., see Langelaar (2018) and Krol et al. (2012)).

16.2.3   Metamaterials

"Batch-size-indifference" and "complexity-for-free" are the two essential features offered by AM that could be exploited to develop novel types of "designer" materials (Zadpoor, 2017, 2018). Such types of designer materials, which are also referred to as metamaterials, are architected and often lattice-based structures that may exhibit unusual properties originating from their small-scale shape (Zadpoor, 2016). One of these remarkable properties is the possibility for a negative Poisson's ratio (auxeticity) (Kolken and Zadpoor, 2017), which leads to lateral expansion upon longitudinal stretching. A wide range of other properties can be also achieved through the rational design of metamaterials, such as shape morphing (Mirzaali et al., 2018a; van Manen et al., 2018; Janbaz et al., 2016), strain rate dependency (Janbaz et al., 2019, 2020), crumpling (Mirzaali et al., 2017a), and action-at-a-distance (Hedayati et al., 2018c).

Metamaterials may also be useful for biomedical applications, in which case they are referred to as "meta-biomaterials." For example, auxetic behavior has been reported in skeletal tissues, such as tendons (Gatt et al., 2015) and trabecular bone. Evidence shows that scaffolds with auxetic behavior may promote neural differentiation by providing mechanical cues to pluripotent stem cells (Yan et al., 2017). Although there is not much evidence as to the advantages of auxetic behavior for improving bone tissue regeneration, a hybrid design of meta-biomaterials (i.e., the rational combination of unit cells with positive and negative values of the Poisson's ratio) may enhance the longevity of orthopedic implants (Kolken et al., 2018). Meta-biomaterials need to have fully open and interconnected pores to ensure the transportation of nutrients and oxygen to the cells (Bobbert and Zadpoor, 2017; Karageorgiou and Kaplan, 2005; Zadpoor, 2015). Lattice structures exhibit lower elastic moduli than the bulk material they are made of, which allows them to match the properties of native tissues, even if they are made from metals. Meta-biomaterials can also be designed using TPMS-based geometries (Bobbert et al., 2017; Al-Ketan et al., 2018; Ataee et al., 2018; Mohammed and Gibson, 2018; Yánez et al., 2018). AM strut-based and sheet-based meta-biomaterials are currently being intensively researched and are believed to hold great promise.

16.2.4   Bio-inspired design

Bio-inspired design is another approach in the design of lattice structures (see Chapter 17 for more information on Bio-inspired Design). Natural cellular materials,

such as bone, cork, and wood enrich the scaffold design libraries (Nam et al., 2004; Bucklen et al., 2008). There are several key design elements in the structures of natural materials. These design elements can be translated into bio-inspired porous materials. An example of natural cellular materials is the cancellous (or trabecular) bone, which is a porous biological material made of hydroxyapatite crystals and collagen molecules formed at several hierarchical levels. The cellular structure of the cancellous bone consists of a connected network of trabeculae in the form of rods and plates (Ding et al., 2018). Trabecular bone can be also seen as a functionally graded material because its porosity distribution exhibits clear spatial patterns. These features can be used for the design of bio-inspired lattice structures.

The bio-inspired aspect is important, particularly in the design of orthopedic implants. When bone defects exceed a critical size, external intervention is necessary to facilitate the healing processes (Bose et al., 2013). The repair of such a critical-size bone defect can be challenging. The current treatment options are the use of either an autograft (patient's own tissue) or an allograft (donated tissue) (Parthasarathy, 2014). However, the application of autografts and allografts is associated with limited availability and medical challenges. The alternative solution is to design biomimetic materials and structures, such as AM lattices. One way to create the geometry of biomimetic lattice structures is to use imaging modalities, such as computed tomography (CT) and magnetic resonance imaging (MRI). Such image-based designs have been widely used for the design of biomaterials aimed for tissue reconstructions (Hollister et al., 2000; Van Eijnatten et al., 2018). Patient-specific implants (Fig. 16.1k), where the implant geometry and dimensions are matched to the anatomy of the patient are also relevant in this regard (Dérand et al., 2012; Jardini et al., 2014; Mohammed et al., 2016).

16.3 Materials

An ever-increasing list of metals can nowadays be processed using the L-PBF technique. In this section, we will review some key categories of materials relevant for the fabrication of metallic lattices.

16.3.1 Biomedical metals and alloys

To be used in biomedical applications, materials need to exhibit good biocompatibility (Gepreel and Niinomi, 2013). Examples of biocompatible metals are titanium (Ti) and its alloys, stainless steels, cobalt-based alloys (e.g., CoCrMo), zirconium (Zr), niobium (Nb), and tantalum (Ta). These materials exhibit good biocompatibility as well as high corrosion resistance and good mechanical properties (Long and Rack, 1998).

Ti and its alloys (e.g., Ti6Al4V) are perhaps the most commonly used biomaterials. Ti6Al4V is very strong and relatively inexpensive, but it exhibits lower ductility than pure Ti (Wauthle et al., 2015a). Ti6Al4V has been widely applied and is approved for medical use. However, there are concerns regarding its biocompatibility because of the

presence of Al and V (Gepreel and Niinomi, 2013). Pure Ti, on the other hand, has lower mechanical properties but higher ductility and is very biocompatible. Stainless steel is also biocompatible, has a lower price than others, and can be easily fabricated by the L-PBF process, but its elastic modulus is higher than Ti6Al4V (Zadpoor, 2019). Ti6Al4V exhibits sufficiently high fatigue strength. However, its fatigue strength is, for example, lower than that of some CoCr alloys (Ahmadi et al., 2018).

The elastic moduli of solid metals are significantly higher than those of bone. To put this into perspective, the range of elastic moduli of cortical and trabecular bones vary between 3 and 30 GPa (Mirzaali et al., 2016b; Rho et al., 1998) and between 0.02 and 2 GPa (Mirzaali et al., 2018b; Goldstein, 1987), respectively. The elastic moduli of Ti6Al6V and CoCrMo are 110 and 210 GPa, respectively (Niinomi, 2003; Long and Rack, 1998). The elastic moduli of metallic biomaterials need to be adjusted to prevent stress-shielding at the bone-implant interface. Introducing porosity and using lattice structures is an effective approach to creating metallic biomaterials with bone-mimicking elastic moduli. Another approach to reducing the elastic modulus of porous structures is the addition of certain elements to the alloys. For example, β-type Ti alloys can be developed by adding β-stabilizing elements (e.g., Ta, Nb, Zr, and Mo), which offer lower elastic moduli. Examples of such alloys are Ti13Nb13Zr (elastic modulus = 79 GPa) (Davidson et al., 1994) and Ti29Nb13Ta4.6Zr (elastic modulus = 55−65 GPa) (Kuroda et al., 1998).

16.3.2 Biodegradable metals

Biodegradable metals are intended to be present in the body only temporarily to support the healing process. AM lattice structures made of biodegradable metals have been recently developed (Li et al., 2020b), including L-PBF porous iron (Li et al., 2018a), L-PBF porous magnesium (WE43) (Li et al., 2018b), and L-PBF porous zinc (Li et al., 2020a). Different types of medical devices can be fabricated from these biodegradable metals. Mg alloys, as an example, have been used in cardiovascular stents (Erbel et al., 2007), bone fixation, and bone screws (Windhagen et al., 2013).

The in vitro rates of biodegradation of pure zinc and its alloys are around 20−300 μm/year (Wen et al., 2018; Hou et al., 2018; Vojtěch et al., 2011; Katarivas Levy et al., 2017). For Fe- and Mg-based biomaterials, the rates may be, respectively, lower than 50 μm/year and higher than 300 μm/year (Li et al. 2014a; Zheng et al. 2014), which are either too low (Fe) or too high (Mg). Mg-based biomaterials may also produce hydrogen gas at a higher rate than can be dealt with inside the host body. Alloying may be used to adjust the rate of biodegradation of biodegradable metals. For instance, Mg-based alloys with elements, such as Y, Sr, Zn, Zr, and Ca have significantly lower biodegradation rates, as compared to pure Mg (Wang et al., 2016). These alloys also exhibit higher strengths, making them suitable for the fabrication of load-bearing parts (Yuan et al., 2019a). Increasing the surface area can tune the biodegradation rate as well. Given that lattice structures have a much larger surface area than corresponding solid parts, they could be used to increase the biodegradation rates of slow-degrading metals, such as iron. AM of biodegradable metals is quite challenging, particularly in the case of magnesium and its alloys, because they are

extremely inflammable and require special safety measures. The biodegradation process may cause cytotoxicity (Li et al., 2015) against human cells, which is why the cytocompatibility of all biodegradable metals should be thoroughly investigated (Zadpoor, 2019).

16.3.3   Shape memory alloys

Shape memory alloys (SMAs) can switch between two permanent shapes when stimulated by external stimuli (Andani et al., 2014). The shape memory effects originate from the temperature-driven phase transformation of SMAs. SMAs have recently made their way to biomedical applications. Typical SMAs include nitinol (NiTi), which contains approximately 50% Ni and 50% Ti by atomic composition. The shape memory behavior of NiTi originates from the change from the austenite phase to the martensite phase in high and low temperatures, respectively (Buehler et al. 1963; Elahinia et al., 2012). The austenitic elastic modulus of bulk nitinol is ≈ 48 GPa, which is significantly lower than that of Ti alloys. Nitinol can also recover relatively large deformations of up to 8%. NiTi SMAs can undergo large strains while maintaining constant stress (Haberland et al., 2014; Morgan, 2004). These characteristics make nitinol an appropriate candidate for medical devices, including surgical guides, stents, orthodontic wires, plates, and staples for bone fracture.

The lattice structures of near equiatomic Ni-Ti alloys are also promising materials for application in the development of bio-implants and biological microelectromechanical systems (bio-MEMS) due to their unique combination of thermal and mechanical shape memories, high corrosion resistance, superelasticity, and biocompatibility (Elahinia et al., 2012; Mitchell et al., 2018). The presence of Ni in NiTi SMAs, however, may raise concerns in biomedical applications, as Ni ranks high in metallic allergy tests (Biesiekierski et al., 2012; Köster et al., 2000). Therefore, surface modification techniques and alternative alloying elements have been proposed (Obbard et al., 2010). For example, TiNb and related alloys (i.e., TiNbX, where X = Zr, Ta, Hf) have been developed, which exhibit recoverable strains of up to ≈ 4.2% (Miyazaki et al., 2006). Ti(C, N) barrier coatings have been applied to NiCr alloys by means of magnetron sputtering to reduce the amounts of nickel and chromium ions released to biologically relevant environments (Banaszek and Klimek, 2019).

Due to high reactivity, low workability, and the strong dependence of their properties on microstructure (Bormann et al., 2014; Van Humbeeck, 2018), manufacturing of parts from SMAs could be quite difficult. AM in general and the L-PBF technique in particular are the promising approaches for the fabrication of lattice structures of SMAs (Speirs et al., 2017; Wang et al., 2018a). The L-PBF technique has been recently used to fabricate lattice structures of NiTi SMAs, particularly for biomedical applications (Hoffmann et al., 2014; Habijan et al., 2013; Haberland et al., 2014; Bernard et al., 2012; Gorgin Karaji et al., 2017). The mechanical properties of L-PBF NiTi SMA parts have been shown to be similar to cast NiTi SMA counterparts (Haberland et al., 2014).

16.3.4 Superalloys

Superalloys are the specific types of alloys, including Co-, Fe-, and Ni-based alloys, that have superior resistance against surface degradation and are able to maintain their mechanical properties at high temperatures and are, thus, attractive options for aerospace, automotive, and energy industries (Kataria et al., 2020). Similar to SMAs, superalloys may also exhibit unusual properties, such as superelasticity (i.e., recover large deformations). Inconel alloys, such as Inconel 100, 625, 718, and 825, are the typical examples of Ni-based superalloys that show superior creep and oxidation resistance, as well as retained mechanical properties at elevated temperatures (Han et al., 2019; Juillet et al., 2018). The L-PBF process provides the opportunity to build lattice structures of superalloys with complex geometries to offer a combination of tailored mechanical properties, light weight, and heat resistance (Leary et al., 2018).

16.3.5 In-situ *alloying and composites*

In-situ alloying refers to the processes that combine several feedstocks with various compositions and simultaneously feed them into the melt pool. Such a compositional mixture can achieve tailored properties and functionalities (Bourell et al., 2017). Examples of such materials include the L-PBF-processed in-situ Ti-26Nb alloys for biomedical applications (Fischer et al., 2016), biofunctionalized Cu-containing titanium alloys (Krakhmalev et al., 2017; Vilardell et al., 2020), and the anchorless L-PBF AlSi12 in-situ alloy that has been developed to mitigate the residual stresses developed during the L-PBF process (Vora et al., 2015).

Generally, reinforcing particles (mostly ceramics) or *in-situ* alloying elements can be added to metal matrices to enhance the mechanical properties of the processed materials including their hardness, stiffness, and strength, while benefiting from the intrinsic properties of the matrix materials, such as high toughness and/or electrical/thermal conductivity. Reinforcing particles can be added through *ex-situ* mixing methods, such as ball milling, or be formed in-situ during the AM processes by combining the metal matrix with the alloying elements. The processing parameters used in the L-PBF processes, such as laser power, must be adjusted to ensure the complete melting of the metal matrix and the alloying elements, to improve the interaction with the surrounding *ex-situ* added particles, or to achieve the maximum reaction between the matrix and the alloying elements. For instance, Ti-TiB porous composites have been fabricated through *in-situ* reaction between the Ti matrix and TiB2 reinforcing particles (Attar et al., 2015). The concept of porous metal-matrix composites is not restricted to *ex-situ* or *in-situ* metal-ceramic composites. It is also possible to fabricate porous metallic glass composites through the L-PBF process. The reinforcing agents in such composites are the crystalline phases distributed in the porous amorphous matrix (Liang et al., 2020). The capabilities of the L-PBF process to fabricate various metal matrix composites has been demonstrated in the

literature (Zhang and Attar, 2016; Zhao et al., 2019; Mandal et al., 2020; Attar et al., 2014), indicating the excellent opportunity to take advantage of both abilities of these processes (i.e., compositing and lattice structure formation) to build lattice structures that are reinforced by composite elements. Functionally graded lattice structures with a gradient of chemical composition can be also created.

16.4   Process-related effects

While AM processes, particularly the L-PBF process, are capable of fabricating lattices with complex geometries, the quality of the resulting structures significantly depends on the processing parameters (Wang et al., 2013). Some of the important processing parameters include laser beam power density, laser spot size, laser scanning speed, focal offset distance, scanning strategy, and build-plate preheat temperature (Gokuldoss et al., 2017; Wang et al., 2016) (see Chapter 3 for more information). In order to manufacture uniform, reproducible, and reliable AM lattices, these parameters should be controlled and adjusted. Therefore, several design maps have been proposed in the past to help in the proper identification and selection of AM-related processing parameters (Beuth et al., 2013; Beuth and Klingbeil, 2001; Gockel and Beuth, 2013).

16.4.1   Effects of processing parameters on internal porosity and microstructure

Inappropriate selection of the processing parameters can create defects, such as microporosities, during the AM processes (Fig. 16.2a−e). The formation of microporosities highly depends on the density of the energy transferred to the melting material, because it directly affects gas/flow interactions and temperature evolution during the AM process (see Chapter 6 for more information). It should, however, be noted that the energy density alone cannot explain all the effects of the processing parameters and the processing parameters should be individually optimized. When using the L-PBF process, there are multiple processing windows within which a minimum number of pores can be achieved in lattice structures (Cosma et al., 2020; Du Plessis et al., 2020; Salem et al., 2019; Sing et al., 2018), see Chapter 3. As a rule of thumb, low power densities increase the microporosities due to insufficient melting. On the other hand, at high laser power densities keyhole pore formation happens, and it may make the melt pool more turbulent, with intensive spattering, evaporate alloying elements, entrap inert gas, and form gas bubbles that become entrapped as the material resolidifies. Moreover, increasing the hatch spacing and thickening the powder layer result in unwanted porosities, especially in the case of thick struts (due to insufficient melting and bonding) (Zhang et al., 2019). Such undesired porosities influence the functionality of the struts and may adversely affect their mechanical performance. Moreover, unmolten particles and spatter melts increase the surface roughness of struts, which may also deteriorate their mechanical performance, particularly their fatigue life.
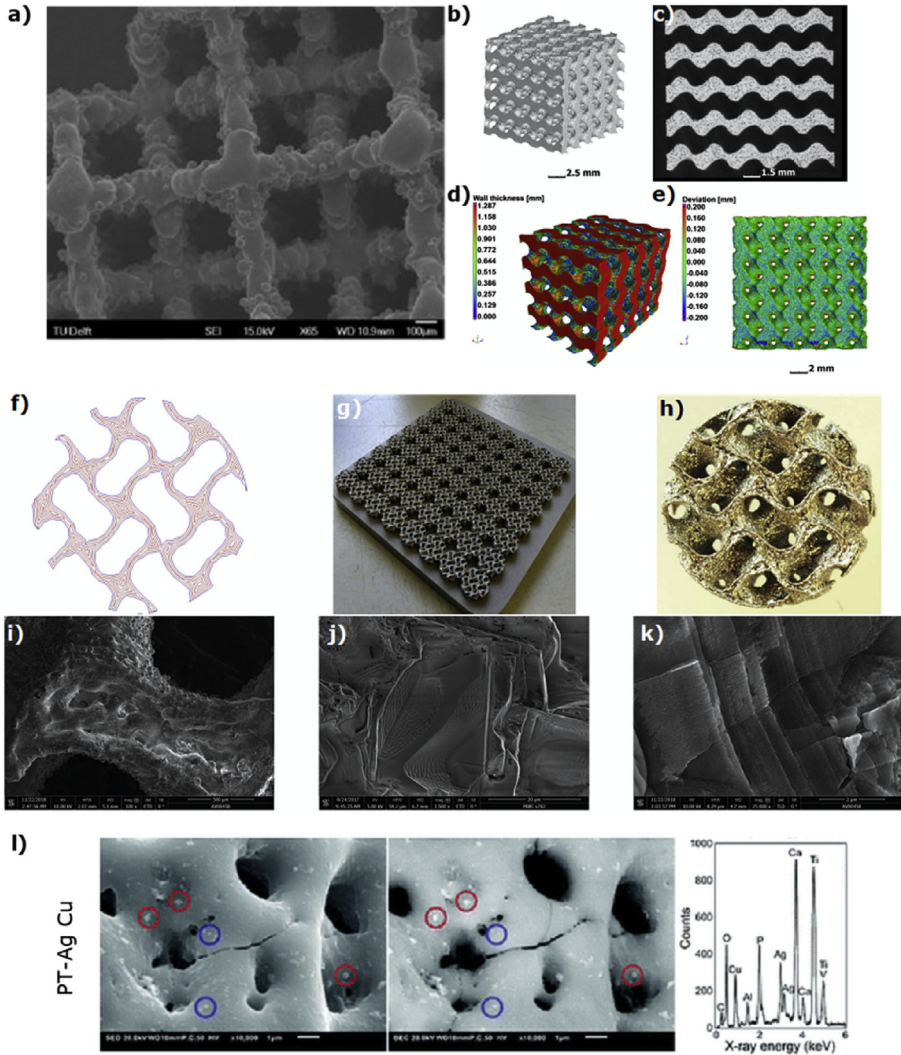
Figure 16.2 AM processing parameters affect the formation of geometrical irregularities (a) or the micro-porosities present in the struts of lattice structures (b, c). Nondestructive imaging techniques, such as CT can be used to quantify the morphological variations (d, e). Various post-AM surface treatments can be used to introduce additional functionalities to lattice structures (e.g., biofunctionalities). The post-AM treatments can be through layer-by-layer approaches (Yavari et al., 2020) (f−k) or adding specific agents (e.g., silver and copper nanoparticles) to activate self-defending abilities of AM lattice-structured biomaterials (van Hengel et al., 2020) (l).
(a) Reprinted from Campoli et al., 2013. Copyright (2020), with permission from Elsevier.
(b−e) Reprinted from Du Plessis et al., 2020. Copyright (2020), with permission from Elsevier.

For instance, it has been observed that for laser powers between 170 and 350 W, energy densities higher than 8 J/mm^2 worsen the surface quality of struts in AlSi10Mg lattice structures while energy densities below 2 J/mm^2 bring about unmolten particles and internal porosities to the extent that they prevent the successful manufacturing of such structures (Großmann et al., 2019). Even for a constant value of the energy density, changes in other individual processing parameters can influence the print quality (Ghouse et al., 2017). That is why energy densities alone without specifying other process parameters cannot be a process indicator and are unable to capture the complex physics of the melt pool (see Chapters 3 and 4).

The actual strut thickness depends on the processing parameters too. Moreover, any changes in the processing parameters affect the thermal history of the melt pools, and, thus, the microstructure of lattice structures. The volume fraction of each phase highly depends on the processing routes and process parameters (Chapter 8). Since microstructure is one of the most important factors determining the mechanical properties of lattice structures, the specification of the applied L-PBF process strongly affects the microstructure and functional properties of lattice structures (Ghouse et al., 2017).

16.4.2   Effects of strut orientation

The manufacturing quality of the struts within a lattice structure is dependent on their orientation with respect to the building direction. Horizontal or near horizontal struts may be associated with some difficulties, including uneven distribution of material during layer deposition, overhang of accumulated molten material, and, thus, localized waviness within the struts (Wauthle et al., 2015c; Campoli et al., 2013). Such an inhomogeneous distribution of material can generate sharp notches on the struts, which are prone to failure and decrease the fatigue life of the lattice structures (Dallago et al., 2019). The orientation of struts can also introduce anisotropy into the mechanical behavior of metallic lattices (Kok et al., 2018).

The orientation of struts or unit cells with respect to the direction, along which the mechanical load is applied (defined by the parameter θ) influences the fatigue properties of the porous structures, because the apparent relative density of such structures is determined by this structural parameter. This influence has been studied in the case of Ti6Al4V octahedral structures. In these structures, the optimized fatigue life per unit density is obtained when $\theta = 43°$ (Bai et al., 2020). The mechanical properties of the lattice structure can, therefore, be adjusted by changing the orientation of unit cells.

16.4.3   Chemical composition

The chemical composition of the powder material governs the possible phase transformations during the AM process as well as the final microstructure and mechanical properties of the resulting lattices. The presence or absence of any alloying elements may also influence the outcome. For instance, the addition of Nb or V to Ti enhances the stability of the β phase and restricts the β to α' (martensite) transformation (Wang et al., 2017a). As a result, the final lattice structure may show better ductility. Moreover, adding large amounts of interstitial atoms, such as O, N, and C, causes some

titanium-based cellular structures to behave like brittle materials with no plateau regions in their stress-strain curves. Such impurities may arise from the initial powder bed or be due to oxygen pickup during the AM process. As a result, it is necessary to control the amounts of such impurities, for example, by using an inert atmosphere with high purity. The addition of pore-inducing agents to the chemical composition of raw powders can also enhance the pore formation during the AM processes and lead to lighter porous parts. Therefore, this effect should also be kept in mind in the design process. To date, most of the research on the chemical compositions of the materials fabricated by the L-PBF process has been restricted to bulk specimens.

16.5   Morphological properties

One of the requirements of a successful AM process is that the geometry of the 3D printed part should match the CAD design (geometrical fidelity). Geometrical imperfections can drastically reduce the mechanical properties (e.g., fatigue properties) of AM lattice structures. Statistical quantification of the discrepancies between the as-designed and as-built geometries is of critical importance (Brajlih et al., 2011). There are (at least) two types of defects in AM parts, including irregularities on the cross-section of the struts (Fig. 16.2a) and the formation of microdefects (Campoli et al., 2013) (Fig. 16.2b and c). The factors that influence the morphological variations are: (a) the complexity of the geometry, (b) the processing parameters, and (c) the local variations of the thermal properties of the system (El Elmi et al., 2020; Li et al., 2017). There are several methods that can be used for nondestructive measurement of the morphological properties of lattices, including optical and confocal microscopies, scanning electron microscopy (SEM), and microcomputed tomography (μCT) (Fig. 16.2d and e).

In order to quantify the morphological characteristics of lattice structures, nondestructive imaging techniques can be used. The spatial resolution of the images (i.e., voxel size) should be equal or better than the minimum feature size that the imaging technique needs to capture. Several steps, including image reconstruction, image filtering (noise removal), and image segmentation, are necessary for image analysis. There are various tools and software (e.g., ImageJ (Abràmoff et al. 2004) and BoneJ plugin (Doube et al., 2010)) that can be used to extract this morphological information from images.

16.5.1   Porosity

There are two types of porosities in AM lattice structures. The first type (microporosities) refers to the microporosities formed within the material. The second type refers to the porosity of the lattice structure (porous structure) as a whole. Microporosities may be in the range of $10-50$ μm (Vilaro et al. 2011), while the pores of AM lattices are

usually >100 µm. Microporosities can act as stress concentration zones and can promote crack propagation, thereby reducing the mechanical properties of AM lattices (Azarniya et al., 2019; Ahmed et al., 2019).

16.5.2   Pore characteristics

Pores are some of the most important morphological features of lattice structures and are described using a host of qualitative and quantitative factors, including pore shape, pore size, strut thickness, pore spacing, connectivity of the unit cell, and the connectivity of the overall lattice structure. The pore size and distribution are among the main indices describing the geometry of lattice structures. The morphology and microstructural characteristics of pores can be measured using optical microscope, SEM, transmission electron microscope (TEM), and atomic force microscopy (AFM) (see Chapter 6 for more details). The 3D shape of pores can be measured using µCT (in addition to the above-mentioned characteristics). Controlling the geometrical features of lattice structures allows one to achieve specific mechanical and physical properties. For example, by controlling the shape, distribution, and interconnectivity of the pores of a lattice structure (or other porous materials), it is possible to adjust the mass transport properties (e.g., permeability) of tissue engineering scaffolds (Bobbert and Zadpoor, 2017; Bobbert et al., 2017; Van Bael et al., 2012; Zadpoor, 2015) and increase their surface area-to-volume ratio (Ahmadi et al., 2014).

16.6   Post-processing

The as-built AM lattice structures often contain defects in the form of microcavities in individual struts, for example, due to lack of fusion (LOF) or other pore types (see Chapter 6 for more details). The presence of these process-induced defects may introduce considerable variations into the mechanical properties of AM lattices structures. Several post-processing treatments, such as heat treatments at high temperatures combined with increased pressures, can be used to eliminate or modify such (microstructural) imperfections. Post-processing can also reduce the residual stresses present in the as-built L-PBF parts (see Chapters 9 and 12).

16.6.1   Residual stress relieving

Due to the thermal gradients experienced during AM, residual stresses develop in lattice structures (Hussein et al., 2013). The amount of residual stresses depends on the thermal history experienced during the AM process. These residual stresses can adversely affect the mechanical performance and geometrical fidelity of AM (Maconachie et al., 2019). Post-processing can reduce the thermal stresses in AM parts. For example, stress relief treatments may be used to transform the microstructure of AM Ti6Al4V lattice structures from acicular martensite α' to the alpha phase (Huang et al., 2020). This phenomenon is concurrent with the elimination of printing-induced residual stresses and a reduction in the cracking tendency, resulting in a significant improvement in the fatigue behavior of post-processed AM materials (Huang et al., 2020).

16.6.2 Heat treatments

Heat treatments are used for improving the microstructures resulting from the L-PBF process (Chapter 8). These treatments can influence the grain size and precipitates (Brandl and Greitemeier, 2012; Song et al., 2014). As an example, post-AM heat treatment of Ti6Al4V parts at temperatures higher than the β transus temperature (i.e., $T_β = 995\ °C$) can thoroughly dissolve the α-phase while coarsening the prior-β grains (Vrancken et al., 2012). A successful heat-treatment process can also improve the mechanical properties of AM lattice structures, such as L-PBF Ti6Al4V (Thöne et al., 2012). Such improvements in the mechanical properties are a direct consequence of microstructural changes and the elimination of thermal stresses.

16.6.3 Hot isostatic pressing (HIP)

HIP is a common post-processing treatment that combines high temperatures with high pressures to decrease or eliminate the internal pores present inside AM parts (Ahmadi et al., 2019; Tammas-Williams et al., 2016; Van Hooreweder et al., 2017). Implementing the HIP process can improve the ductility of AM materials (Zadpoor, 2019), increase the quasi-static mechanical properties of AM meta-biomaterials (Ahmadi et al., 2019), and decrease the degree of anisotropy present in metallic lattices (Wu and Lai, 2016).

However, the role of the HIP treatment in influencing the fatigue behavior of AM lattice structures remains controversial. Some studies have reported no improvement of the fatigue life for AM lattice structures made of Ti6Al4V (Dallago et al., 2018) and CoCr alloy (Cutolo et al., 2018). This can be explained by the fact that HIP treatment cannot fix the defects (e.g., strut thickness variations, strut waviness) presented on top surfaces (Dallago et al., 2018). These defects are the preferred zones for crack initiation. In the case of Ti6Al4V lattice structure, it is shown that HIP at $1000°C/150\ MPa$ decreases the microhardness by 20%, the yield strength by 30%, and increases the fatigue endurance ratio at 10^6 cycles by 83% through removing the pores present in the struts and the phase transformation of brittle α'-martensite to tough α + β mixed phases. The coarser α + β mixture can blunt the fatigue cracks, thereby decelerating their propagation and improving the fatigue performance of the material (Wu et al., 2017b; Huang et al., 2020).

16.6.4 Surface treatments

Several types of surface treatment processes have been proposed for (metallic) lattice structures. One approach to smoothen the external surface of struts is physical erosion by using abrasive materials. An example of such techniques is sandblasting, which can remove the excess powder particles adhered to the surface of struts, introduce compressive residual stresses to their superficial regions, and form a nanocrystalline thin film covering the outer regions of the struts. These changes can enhance the endurance limit of AM lattices (Yang et al., 2019). However, the abrasive materials may not reach the internal struts of lattice structures. Another method to modify the surface roughness of struts is chemical etching, which can better reach the internal struts.

However, chemical etching may not always improve the fatigue performance of lattice structures. For example, while chemical etching is reported to improve the fatigue behavior of Ti6Al4V lattices, the opposite has been reported for CoCr (Van Hooreweder and Kruth, 2017). One of the reasons is that too much material may be removed during such a process.

Chemical surface treatments can have different influences on the fatigue properties of AM lattices. In general, there are two types of chemical surface treatments: light chemical surface treatments that are used to remove the unmolten powders from the strut surfaces, and chemical surface treatments for inducing specific (bio-)functionalities (Fig. 16.2f−l). Some chemical surface treatments applied for biofunctionalization (Fig. 16.2f−l) have been shown to improve the fatigue properties of the materials as well (Cutolo et al., 2018). There is also some evidence that certain biofunctionalizing surface treatments, such as alkali-acid heat treatment (Yavari et al., 2014a) and plasma electrolytic oxidation (Karaji et al., 2017), do not affect the fatigue lives of AM lattices. Combining HIP with surface treatments, such as sandblasting and chemical etching, however, has been shown to further improve the fatigue lives of AM lattices (Ahmadi et al., 2019).

In the case of AM meta-biomaterials, those include surface bio-functionalization processes that enhance the tissue regeneration performance of such materials (Yavari et al., 2014b; Nune et al., 2018; Van Der Stok et al., 2015b; Nouri-Goushki et al., 2019) and prevent implant-associated infections (Geng et al., 2017; Amin Yavari et al., 2016; van Hengel et al., 2017; Ganjian et al., 2020). This can be achieved through chemical and electrochemical surface treatments and coatings. Some of those surface treatment processes may, however, decrease the mechanical properties of AM lattices as they erode struts and make them rougher.

16.7 Physical properties

16.7.1 Density

The relative density (ρ) of AM lattice structures refers to the amount of solid constituent that fills the nominal volume of the porous body. The relative density or porosity ($= 1 - \rho$) is among the key parameters determining the mechanical and physical properties of lattice structures. The relative density of a porous structure can be measured using the Archimedes' principle or through the analysis of microscopic or μCT images (see Chapter 10 for more details). The relative density of a designed object can also be calculated from the CAD design. The mismatches between the "designed" and "measured" densities can be due to the formation of (geometrical) defects and the irregularities caused by the AM process.

16.7.2 Surface roughness

Surface roughness is one of the most important features affecting the quality of AM lattices. Several factors can influence the surface roughness of AM lattice structures,

including the quality of the feedstock material (Tang et al., 2015a). Moreover, unmolten powder particles and the occurrence of the balling effect during the L-PBF process can increase the surface roughness (Gu and Shen, 2009; Niu and Chang, 1999). Unmolten particles, which may result from an inadequate level of energy input, stick to the surface of the struts of lattice structures and roughen the surface. The third parameter influencing the surface quality is the build rate, with higher build rates leading to poorer surface quality, which may necessitate post-AM treatments, such as chemical polishing, shot peening, or HIP (Łyczkowska et al., 2014; Alghamdi et al., 2019). Nondestructive imaging techniques, such as SEM and surface profilometry, can be used to assess the surface roughness (Strano et al., 2013).

16.8 Mechanical properties

A wide variety of materials, process type, process parameters, and design factors significantly influence the quasi-static mechanical properties and fatigue properties of the lattice structures made through L-PBF. Whether the microstructure of the material constituting the struts is isotropic or anisotropic may also considerably affect the mechanical properties. In order to establish a reliable relationship between the design of the repeating unit cell and the "effective" mechanical properties of a lattice structure, the lattice structure should contain a minimum number of unit cells (i.e., the minimum number of unit cells is 10 unit cells, as proposed in ISO13314). The mechanical properties of functionally graded porous structures are, as expected, strongly size-dependent. Comparing the mechanical properties of graded designs with those of uniform structures has shown higher elastic moduli (Wang et al., 2018b) and energy absorption capacities (Choy et al., 2017) of functionally graded lattice structures.

16.8.1 Quasi-static mechanical properties

The mechanical properties of lattices (i.e., the elastic modulus, E, and yield strength, σ_y) depend on their geometrical and physical features and follow a power-law relationship $E = a\rho^b$, where ρ is the relative density (Ashby, 2006; Gibson and Ashby, 1999) (Fig. 16.3a and b). The coefficients of the power-law (i.e., a and b) depend on the geometry of lattice structures (Hedayati et al., 2016c, d). For example, b is close to 1 for stretch-dominated unit cells, while it tends to be closer to 2 for bending-dominated unit cells (Ashby, 2006; Deshpande et al., 2001b).

The differences between the estimated mechanical properties (i.e., using computational modeling) and those predicted by the power-law relationship often originate from the presence of the residual stresses created during the L-PBF process (Wang et al., 2017b; Yan et al., 2014), uncertainties in the exact geometry of the struts (Zhang et al., 2018), and the overestimation of the relative density when using the Archimedes technique (Yakout et al. 2019). One of the possible reasons for such an overestimation is the presence of unmolten powder particles on the surface of the struts.
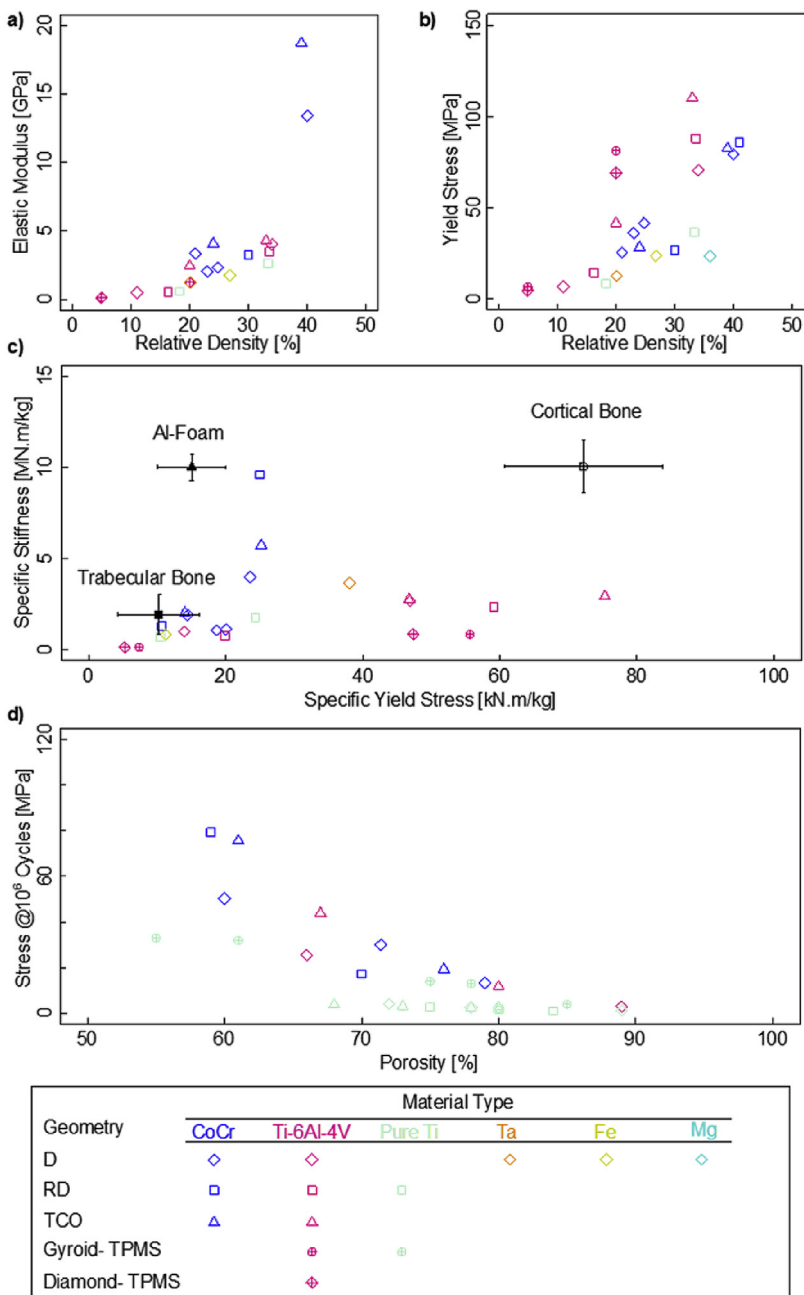
Figure 16.3 The mechanical properties (elastic modulus (a) and compressive strength (b)) of L-PBF lattice structures as a function of their relative densities. The data were collected for CoCr (Hedayati et al., 2018a; Cutolo et al., 2018), Ti-6Al-4V (Ahmadi et al., 2014; Ge et al., 2020; Yan et al., 2015), pure titanium (Ti) (Wauthle et al., 2015a), tantalum (Ta) (Wauthle et al., 2015b), iron (Fe) (Li et al., 2018a), and magnesium (Mg) (Li et al., 2018b). The specific mechanical properties (i.e., the ratio of the elastic properties to the density of porous structures) are compared with those of natural materials (e.g., cortical (Carter and Spengler 1978; Mirzaali et al., 2016b; Mirzaali et al., 2015) and trabecular (Goldstein 1987; Mirzaali et al., 2018b; Mirzaali et al., 2017c; Mirzaali et al., 2020) bone) and aluminum foams (Andrews et al. 1999; Miyoshi et al., 2000; Mirzaali et al., 2016a). The endurance limit values at 10^6 cycles versus

To exclude the effects of the material type, the mechanical properties can be normalized with respect to the mechanical properties of the bulk material from which the struts are made. However, it has been recently shown that these normalized values of the elastic modulus and yield stress can significantly change with the type of the material (Hedayati et al., 2018a) (Fig. 16.3a and b). Moreover, different metals have different ductility levels and, thus, different post-yield behaviors. For example, changing the bulk material may influence the plateau stress and densification behavior at the start of the self-contact of struts in lattice structures (Hedayati et al., 2018a). Despite the presence of such effects, the normalized values of the quasi-static mechanical properties of AM lattices are more strongly affected by the geometrical design of the lattice structures than the material type (Hedayati et al., 2018a; Zadpoor, 2019).

Microscale measurements of the full field strain during the mechanical testing of AM lattices have shown that the failure of AM lattices is caused by strain concentrations in the weak spots formed during the AM process (Genovese et al., 2017). The strain concentrations intensify as the loading progresses and lead to premature failure. While the microscale failure mechanism of AM metallic lattices seems to be independent of their geometrical design (Genovese et al., 2017), the geometrical design significantly influences the macroscale failure mechanisms of AM lattices (Kadkhodapour et al., 2015; Ahmadi et al., 2014). In particular, the failure mechanisms of stretch-dominated unit cells differ from those of bending-dominated unit cells (Kadkhodapour et al., 2015). In stretch-dominated unit cells, entire rows of unit cells collapse as the struts and joints in stretch-dominated structures are highly stiff and do not bend under axial loads (Deshpande et al., 2001b). In contrast, the struts of bending-dominated structures can easily rotate at their joints under macroscopically applied loads, leading to their overall collapse (Bauer et al., 2014). Therefore, in bending-dominated unit cells, 45° shearing bands and the consequent propagation of cracks are responsible for the failure of lattice structures (Kadkhodapour et al., 2015). The local buckling of individual struts is another failure mechanism involved in the overall failure of AM lattices, and may lead to a more brittle mechanical behavior (Li et al., 2014b).

There are some distinct differences between the typical stress-strain curves of bending-dominated and stretch-dominated lattice structures. Bending-dominated cellular structures exhibit a linear elastic behavior up until the end of their elastic region, where the walls or edges of the unit cells start to yield, buckle, or fracture, after which the integrity of the lattice structure is compromised around the plateau stress, σ_{pl}, and densification strain, ε_d. In contrast, stretch-dominated lattice structures

the porosities of the LPBF-lattice structures made of Ti-6Al-4V (Yavari et al., 2015) and CoCr (Ahmadi et al., 2018; Van Hooreweder and Kruth, 2017) and Ti (Zargarian et al., 2016; Kelly et al., 2019) (D). Wherever possible, the data for different beam-based unit cells types, such as diamond (D), rhombic dodecahedron (RD), and truncated cuboctahedron (TCO) and sheet-based unit cells, including TPMS-gyroid and TPMS-diamond, were added.

benefit from a higher strength and elastic modulus, but undergo post-yield softening. As expected, the biodegradation process can reduce the mechanical properties of AM lattice structures in the case of biodegradable metals. This effect has been observed to be more severe for the yield stress than for the elastic modulus (Li et al., 2018a, b).

16.8.2   Fatigue life

The fatigue life of AM lattices is an important consideration for most of load-bearing applications, including orthopedic implants that are often subjected to repetitive loading due to the physical activities of the human body. Given the importance of the biomedical applications of AM lattices, compression-compression fatigue is one of the most well-studied types of the fatigue loading modes applied to AM lattices. However, the other types of fatigue loading, such as tension and bending, are also highly consequential. A macroscopically applied compression-compression load may lead to the development of tensile stresses in the struts of AM lattice structures, thereby promoting crack initiation and eventual strut failure. Several studies on the compression-compression fatigue behavior of AM lattices made from different metals have in recent years appeared in the literature (Ahmadi et al., 2018; Van Hooreweder et al., 2017; Yavari et al., 2013, 2015; Speirs et al., 2017). The S-N curves determined in such studies show the number of cycles to failure for different levels of the applied stress. The endurance limit or fatigue strength is defined as the stress at which the number of loading cycles exceeds a specific threshold (e.g., 10^6 cycles). The fatigue strengths of lattice structures increase with the fatigue strength of the bulk materials of the same composition (Zargarian et al., 2019) (Fig. 16.3d).

Geometrical variables, such as the relative density and unit cell type, are also important in this regard (Fig. 16.3d). The fatigue strength of lattice structures decreases as the porosity increases (Yavari et al. 2013, 2015). Several normalization approaches have been proposed in the past to eliminate the effects of the quasi-static mechanical properties from the dynamic properties and define the so-called "normalized S-N curves." One of those approaches is to divide the stress levels by the yield or plateau stress of the lattice structure. For Ti6Al4V, the S-N curves of lattice structures with different values of the relative density but the same type of unit cell tend to collapse into one curve once they are normalized with respect to the their quasi-static mechanical properties (Yavari et al., 2013). This observation seems to be approximately (but not exactly) valid for some other alloys as well (Ahmadi et al., 2018). The use of a single normalized S-N curve is a powerful idea that has a huge time- and cost-saving potential. That is because to apply a normalized S-N curve to a new lattice structure (of the same unit cell type), one only needs to determine the plateau or yield stress by conducting a limited number of quasi-static mechanical tests.

The tensile fatigue behavior of AM lattice structures has been also studied (Dallago et al., 2018; Lietaert et al., 2018). The fatigue performance of AM lattices decreases under tension-tension as compared to compression-compression loading (Lietaert et al., 2018). The tension-compression loading, however, tends to increase

the fatigue lives of AM lattices because, as opposed to tension-tension and compression-compression loading modes, a smaller number of struts experience local tensile stresses.

The geometrical design of AM lattice structures (i.e., unit cell types) significantly influences their fatigue behavior (Yavari et al., 2015; Zhao et al., 2016) (see Fig. 16.3d for comparison). In compression-compression fatigue, the geometry of the unit cell determines how much of the macroscopically applied compressive loading is experienced as tensile stresses by the struts. Sheet-based lattice structures tend to outperform strut-based lattices in terms of their fatigue resistance (Bobbert et al., 2017). This is due to two reasons. First, sheet-based lattices are less sensitive to the defects and irregularities caused by the AM process. Second, due to the continuity of their unit cells, no stress concentration points exist in sheet-based lattice structures (Lietaert et al., 2018). The fatigue behavior of AM lattices with disordered geometries needs to be further investigated. As for functionally graded lattice structures, they have been found to cause a continuous redistribution of stresses due to their inhomogeneous microstructural arrangements (Zhao et al., 2018).

In addition to geometrical design, the material type plays an important role in determining the fatigue life of AM lattices, particularly in the high cycle regime (see Fig. 16.3d for comparison). Depending on the geometrical design and material type, the fatigue strengths of most (strut-based) AM metallic lattices range between 20% and 60% of their yield strengths (Ahmadi et al., 2018). Examples of the related properties that could improve the fatigue strength of AM lattices are ductile mechanical properties (e.g., the relatively high ductility of pure titanium (Wauthle et al., 2015a) and superelasticity (e.g., of β-type titanium alloys (Liu et al., 2017)). The L-PBF process can also create anisotropy in the fatigue behavior and other mechanical properties of lattice structures (Kajima et al., 2016). Further studies are, therefore, needed to determine the relationship between the fatigue behavior and build orientation of AM lattice structures. A recent review of fatigue performance of lattice structures is found in (Benedetti et al., 2021).

16.9 Computational modeling and analytical solutions

Predictive models in the form of computational models (Campoli et al., 2013; Hedayati et al., 2016c; Du Plessis et al., 2018a) and analytical solutions (Zadpoor and Hedayati, 2016; Hedayati et al., 2017; Hedayati et al., 2016d) can be used to better understand the roles of geometrical design, microstructure, and manufacturing defects in determining the effective properties of lattice structures. Such models can also be used in heuristic algorithms that determine the optimal design of lattices to achieve the desired properties under a specific loading scenario.

The analytical solutions for strut-based unit cells are usually based on the Euler-Bernoulli or Timoshenko beam theories. The relationships between the geometrical

design and mechanical properties for various unit cell types have been established. One of the limitations of the analytical solutions based on the Euler-Bernoulli beam theory is that they are only valid for unit cells with slender struts (i.e., low relative densities) and deviate from experimental results and the results obtained from computational models for the higher values of the relative density (Zadpoor and Hedayati, 2016). The Timoshenko beam theory offers a better performance for thick struts. However, exact solutions based on the Timoshenko theory are only available for a few geometries. One of the limitations of analytical solutions is that they cannot take the geometrical imperfections of the strut shapes into account. To improve the accuracy of analytical solutions, the relative density of the lattice structures should be accurately calculated taking account of the 3D shape of the struts at the junctions (Lozanovski et al., 2020). Ignoring the 3D shapes of the struts and junctions leads to mass multiple counting in the traditional models of lattice structures that model the struts as two-dimensional (2D) lines (Hedayati et al., 2016b; Zadpoor and Hedayati, 2016). Despite their lack of accuracy, analytical solutions offer unique insights into the mechanical behavior of AM lattices and the effects of various design parameters on mechanical properties.

Computational models can also be used to predict the geometry-property relationships of AM lattices. Computational models based on high-fidelity finite element (FE) models can offer more accurate results than analytical models (Campoli et al., 2013). Different elements, such as solid, shell, and beam (based on the Euler-Bernoulli or Timoshenko formulations) elements can be employed in the FE modeling of lattice structures. The idealized geometry, as well as the actual geometry that includes the imperfection and defects imposed during the AM processes, can be used in such FE models. An example of the actual geometry can be constructed from the segmented μCT images (Cho et al., 2015; Youssef et al., 2005; Du Plessis et al., 2017). Computational models can be combined with optimization algorithms to optimize the design of lattice structures for specific applications (e.g., patient-specific implants) under a specific set of loading conditions. One example of such optimization algorithms is the models based on bone tissue adaptation (Arabnejad Khanoki and Pasini, 2012; Lin et al., 2007; Wang et al., 2016).

Computational models could also predict the fatigue behavior of AM lattices. This is important as collecting the data required for establishing experimental S-N curves of lattice structures is extremely expensive and time-consuming. The computational models proposed to date usually use the S-N curves of the base materials, damage evolution laws, and iterative solutions to predict the fatigue lives of lattice structures (Hedayati et al., 2016a, 2018b; Zargarian et al., 2016). These models can be combined with other characterization techniques, such as digital image correlation (DIC) (de Krijger et al., 2017) or *in-situ* imaging (Du Plessis et al., 2018b), to validate the predicted strain distributions and to explore the mechanisms responsible for the local or global failure of lattice structures.

16.10 Applications

16.10.1 *Light-weight and load-bearing structures*

The high porosity and tailored mechanical properties of AM lattice structures make them attractive options for the design of light-weight and load-bearing structures in various industries, including the automotive, civil, energy, and aerospace industries (Fig. 16.4a). Some examples are fairings, payload adapters, and space telescopes in aerospace engineering, submarine bodies in maritime engineering, and sandwich composites in civil engineering (Nagesha et al., 2020). A more specific example is the lattice sandwich structures fabricated by L-PBF, whose application as light-weight thermal controllers has been shown to increase the thermal capacity by up to 50%. Such controllers are used in spacecraft to control the temperature of various electronics (Zhou et al., 2004).

In the automotive industry, light-weight lattice structures are used for noise reduction, better recyclability, and reduced fuel consumption. A 10% decrease in the weight of the structural parts of an automobile delivers a 6%−8% of saving in fuel consumption (Nagesha et al., 2020) (partially due to the snowball effect). Moreover, the natural frequencies of lattice structures increase with their stiffnesses, making them suitable for application in fast motors and vibratory components. Moreover, due to the low weight and good mechanical properties of strut-based lattice structures, they can be
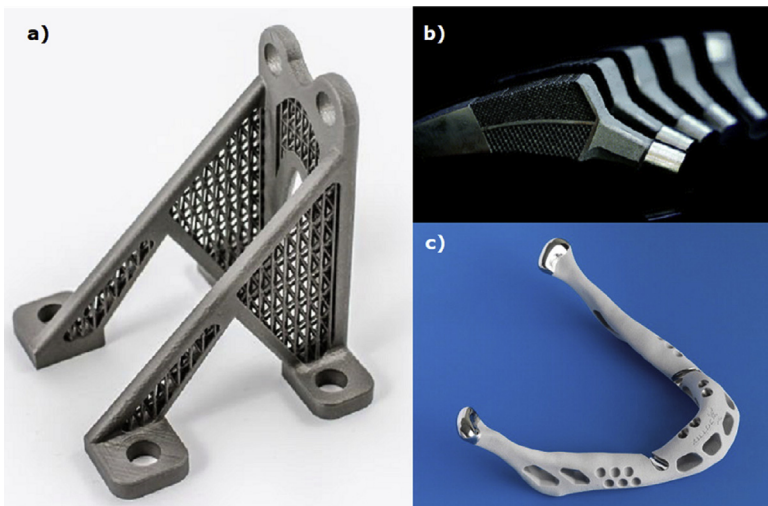
Figure 16.4 AM lattices have several applications in load-bearing lightweight structures particularly for aerospace engineering. This example is an optimized bracket designed by Materialise 3-Matic (reprinted with permission) which exhibits 63% weight reduction (a). Other examples of AM lattice structures include hybrid meta-implants (Kolken et al., 2018) (b) and a patient-specific mandible implant (c).
Reprinted from Nickels, L., 2012. World's first patient-specific jaw implant. Met. Powder Rep. 67, 12−14, Copyright (2020), with permission from Elsevier.

used for the construction of structures located in earthquake-prone areas to prevent subsequent damages, such as fracture, support failure, and local and global buckling (Nagesha et al., 2020).

The relatively high specific stiffness as well as the extended stress plateau of AM lattice structures make them attractive candidates for energy absorption, load-bearing, and impact alleviation applications. The form-freedom offered by the L-PBF process means that it is possible to use novel geometries and periodic patterns that considerably enhance the energy absorption capacity of AM lattices as compared to traditionally fabricated cellular materials (e.g., foams). It has been shown, for example, that auxetic metamaterials offer superior energy absorption capabilities (Yuan et al., 2019b). Moreover, stretch-dominated lattices are known for being able to store more energy than their bending-dominated counterparts (Sun et al., 2020). Using the AM technologies, it is also possible to optimize the internal geometry of parts at several length scales to further enhance their load-bearing capacity (Wang et al., 2018a,b).

In addition to the abovementioned applications, lattice structures can be used in many other areas, such as the design of heat exchangers for chemical processing, waste treatment, thermal management (Maloney et al., 2012), digital signal processing (DSP), digital filtering, spectral estimation, and adaptive signal processing (Roy, 2014).

16.10.2 Biomedical

AM parts in general and AM lattices in particular have found many biomedical applications, particularly in orthopedic (Fig. 16.4b), maxillofacial, and trauma surgeries. Examples include the AM patient-specific mandible implants coated with hydroxyapatite and implanted in a patient in 2012 (Nickels, 2012) (Fig. 16.4c). AM parts have been also applied for the reconstruction of class III cranial defects (Mertens et al., 2013). In addition to porous implants, the L-PBF process can be used to fabricate multifunctional porous medical devices (Bártolo and Bidanda, 2008), controlled drug delivery systems (Burton et al., 2019), and engineered tissues (Putra et al., 2020; Stevens et al., 2008; Gibson et al. 2014).

As extensively discussed elsewhere (Bejarano et al., 2017; Zadpoor, 2019, 2020), there are four main advantages to the use of AM lattice structures as porous biomaterials. First, it is possible to adjust the elastic properties, yield stress, fatigue strength, permeability, diffusivity, and the rate of biodegradation of lattice structures through rational design of their geometries. All these properties of porous biomaterials play important roles in determining the *in vivo* performance of the relevant medical devices. Second, the macroscale shape and microscale architecture of AM lattices can be designed to match the specific anatomy and loading conditions of a specific patient. Third, the surface area of AM lattice structures is much larger than that of a corresponding solid material. The increased surface area of such porous biomaterials could be used for amplifying the effects of surface bio-functionalization treatments, such as those aimed at inducing antibacterial (van Hengel et al., 2017) and osteogenic (Zadpoor, 2019) properties. Finally, the pore space of AM lattices not only allows for

unhindered bony ingrowth but can also be used to accommodate drug delivery vehicles (e.g., those loaded with growth factors (van der Stok et al., 2013, 2015a) and/or antibiotics (Bakhshandeh et al., 2017; Croes et al., 2018; Yavari et al., 2020)) to further enhance the performance of the resulting implants. In addition to these four advantages, researchers continue to develop other innovative ways to exploit the benefits of AM processes.

16.11 Conclusions

To summarize, we reviewed the fundamental aspects of applying the L-PBF process for the fabrication of (metallic) lattice structures as a reference for students and researchers who intend to use this technique. In order to have reliable and reproducible AM lattice structures, special attention must be paid to choosing proper parameters starting from the design steps to the fabrication process and during the post-processing actions.

The design of the geometry of lattice structures is the first step, which determines their overall physical (e.g., permeability) and mechanical properties. There are several classes of geometries that can help designers to make a proper selection. Each of these design classes can provide specific properties.

The L-PBF process parameters have a great influence on the quality of the final parts (e.g., surface roughness, anisotropy, and geometrical fidelity) as well as the formation of defects, all of which can subsequently influence the mechanical performance of AM lattices. The proper selection and adjustment of such processing parameters can minimize unwanted microstructural defects at macro and micro levels.

Several post-processing methods, such as HIP, heat, surface, and chemical treatments can be used to reduce or eliminate some of those defects created during the L-PBF process. Those post-treatments can also introduce multifunctionalities to AM lattice structures (e.g., biofunctionalization) and may strongly influence their (quasi-static or fatigue) mechanical properties. The proper selection of the processing and post-processing parameters highly depend on the material type.

L-PBF lattice structures have found their ways to high-tech industries, such as automotive, aerospace, and biomedical. The research into the development of processing windows and the use of various kinds of materials are some of the active fields expected to grow in the near future.

16.12 Questions

- What are the differences in geometrical and mechanical properties between bending-dominated and stretch-dominated lattice structures?
- What are the important morphological parameters of AM lattice structures?
- What are the most common defects formed during the L-PBF process to fabricate lattice structures?

- How do the L-PBF process parameters influence the morphological and mechanical properties of AM lattice structures?
- How can the post-AM treatment processes (i.e., HIP, heat treatments, surface treatments, chemical treatments) affect the quasi-static and fatigue properties of AM lattice structures?
- What are the main benefits of using disordered AM lattice structures over ordered AM lattice structures?
- What are the main advantages of in-situ alloying in the fabrication of AM lattice structures?

References

Abràmoff, M.D., Magalhães, P.J., Ram, S.J., 2004. Image processing with ImageJ. Biophot. Int. 11, 36−42.

Ahmadi, S.M., Campoli, G., Amin Yavari, S., Sajadi, B., Wauthlé, R., Jan, S., Weinans, H., Zadpoor, A.A., 2014. Mechanical behavior of regular open-cell porous biomaterials made of diamond lattice unit cells. J. Mech. Behav. Biomed. Mater. 34, 106−115.

Ahmadi, S.M., Hedayati, R., Ashok Kumar Jain, R.K., Li, Y., Leeflang, S., Zadpoor, A.A., 2017. Effects of laser processing parameters on the mechanical properties, topology, and microstructure of additively manufactured porous metallic biomaterials: a vector-based approach. Mater. Des. 134, 234−243.

Ahmadi, S.M., Hedayati, R., Li, Y., Lietaert, K., Tümer, N., Fatemi, A., Rans, C.D., Pouran, B., Weinans, H., Zadpoor, A.A., 2018. Fatigue performance of additively manufactured meta-biomaterials: the effects of topology and material type. Acta Biomater. 65, 292−304.

Ahmadi, S.M., Kumar, R., Borisov, E.V., Petrov, R., Leeflang, S., Li, Y., Tümer, N., Huizenga, R., Ayas, C., Zadpoor, A.A., 2019. From microstructural design to surface engineering: a tailored approach for improving fatigue life of additively manufactured meta-biomaterials. Acta Biomater. 83, 153−166.

Ahmed, A.B., Mohamed, I.H., Fathallah, R., Sidhom, H., 2019. The effect of interacting defects on the HCF behavior of Al-Si-Mg aluminum alloys. J. Alloys Compd. 779, 618−629.

Al-Ketan, O., Rowshan, R., Al-Rub, R.K.A., 2018. Topology-mechanical property relationship of 3D printed strut, skeletal, and sheet based periodic metallic cellular materials. Addit. Manuf. 19, 167−183.

Alghamdi, A., Downing, D., McMillan, M., Brandt, M., Qian, M., Leary, M., 2019. Experimental and numerical assessment of surface roughness for Ti6Al4V lattice elements in selective laser melting. Int. J. Adv. Manuf. Technol. 105, 1275−1293.

Amin Yavari, S., Loozen, L., Paganelli, F.L., Bakhshandeh, S., Lietaert, K., Groot, J.A., Fluit, A.C., Boel, C.H.E., Alblas, J., Vogely, H.C., 2016. Antibacterial behavior of additively manufactured porous titanium with nanotubular surfaces releasing silver ions. ACS Appl. Mater. Interfaces 8, 17080−17089.

Andani, M.T., Moghaddam, N.S., Haberland, C., Dean, D., Miller, M.J., Elahinia, M., 2014. Metals for bone implants. Part 1. Powder metallurgy and implant rendering. Acta Biomater. 10, 4058−4070.

Andrews, E., Sanders, W., Gibson, L.J., 1999. Compressive and tensile behaviour of aluminum foams. Mater. Sci. Eng. A 270, 113−124.

Arabnejad Khanoki, S., Pasini, D., 2012. Multiscale design and multiobjective optimization of orthopedic hip implants with functionally graded cellular material. J. Biomech. Eng. 134.

Ashby, M.F., 2006. The properties of foams and lattices. Phil. Trans. R. Soc. A Math. Phys. Eng. Sci. 364, 15−30.

Ataee, A., Li, Y., Fraser, D., Song, G., Wen, C., 2018. Anisotropic Ti-6Al-4V gyroid scaffolds manufactured by electron beam melting (EBM) for bone implant applications. Mater. Des. 137, 345−354.

Attar, H., Bönisch, M., Calin, M., Zhang, L.C., Zhuravleva, K., Funk, A., Scudino, S., Yang, C., Eckert, J., 2014. Comparative study of microstructures and mechanical properties of in situ Ti−TiB composites produced by selective laser melting, powder metallurgy, and casting technologies. J. Mater. Res. 29, 1941−1950.

Attar, H., Löber, L., Funk, A., Calin, M., Zhang, L.C., Prashanth, K.G., Scudino, S., Zhang, Y.S., Eckert, J., 2015. Mechanical behavior of porous commercially pure Ti and Ti−TiB composite materials manufactured by selective laser melting. Mater. Sci. Eng. A 625, 350−356.

Azarniya, A., Garmendia Colera, X., Mirzaali, M.J., Sovizi, S., Bartolomeu, F., Wits, W.W., Yap, C.Y., Ahn, J., Miranda, G., Silva, F.S., 2019. Additive manufacturing of Ti−6Al−4V parts through laser metal deposition (LMD): process, microstructure, and mechanical properties. J. Alloys Compd. 804, 163−191.

Bai, L., Zhang, J., Xiong, Y., Chen, X., Sun, Y., Gong, C., Pu, H., Wu, X., Luo, J., 2020. Influence of unit cell pose on the mechanical properties of Ti6Al4V lattice structures manufactured by selective laser melting. Addit. Manuf. 34, 101222.

Bakhshandeh, S., Gorgin Karaji, Z., Lietaert, K., Fluit, A.C., CHE, B., Charles Vogely, H., Vermonden, T., Hennink, W.E., Weinans, H., Zadpoor, A.A., 2017. Simultaneous delivery of multiple antibacterial agents from additively manufactured porous biomaterials to fully eradicate planktonic and adherent *Staphylococcus aureus*. ACS Appl. Mater. Interfaces 9, 25691−25699.

Banaszek, K., Klimek, L., 2019. Ti (C, N) as barrier coatings. Coatings 9, 432.

Banhart, J., 2001. Manufacture, characterisation and application of cellular metals and metal foams. Prog. Mater. Sci. 46, 559−632.

Bártolo, P., Bidanda, B., 2008. Bio-Materials and Prototyping Applications in Medicine. Springer.

Bauer, J., Hengsbach, S., Tesari, I., Schwaiger, R., Kraft, O., 2014. High-strength cellular ceramic composites with 3D microarchitecture. Proc. Natl. Acad. Sci. 111, 2453−2458.

Bejarano, N.C., Pedrocchi, A., Nardone, A., Schieppati, M., Walter, B., Monticone, M., Ferrigno, G., Ferrante, S., 2017. Tuning of muscle synergies during walking along rectilinear and curvilinear trajectories in humans. Ann. Biomed. Eng. 45, 1204−1218.

Bendsøe, M.P., 1989. Optimal shape design as a material distribution problem. Struct. Optim. 1, 193−202.

Bendsoe, M.P., Sigmund, O., 2013. Topology Optimization: Theory, Methods, and Applications. Springer Science & Business Media.

Benedetti, M., du Plessis, A., Ritchie, R.O., Dallago, M., Razavi, S.M.J., Berto, F., 2021. Architected cellular materials: a review on their mechanical properties towards fatigue-tolerant design and fabrication. Mater. Sci. Eng. R Rep. 144, 100606.

Bensoussan, A., Lions, J.-L., Papanicolaou, G., 2011. Asymptotic Analysis for Periodic Structures. American Mathematical Society.

Berger, J.B., Wadley, H.N.G., McMeeking, R.M., 2017. Mechanical metamaterials at the theoretical limit of isotropic elastic stiffness. Nature 543, 533−537.

Bernard, S., Krishna Balla, V., Bose, S., Bandyopadhyay, A., 2012. Compression fatigue behavior of laser processed porous NiTi alloy. J. Mech. Behav. Biomed. Mater. 13, 62−68.

Beuth, J., Klingbeil, N., 2001. The role of process variables in laser-based direct metal solid freeform fabrication. J. Occup. Med. 53, 36−39.

Beuth, J., Fox, J., Gockel, J., Montgomery, C., Yang, R., Qiao, H., Soylemez, E., Reeseewatt, P., Amin, A., Narra, S., 2013. Process mapping for qualification across multiple direct metal additive manufacturing processes. In: Solid Freeform Fabrication Proceedings. University of Texas, Austin, pp. 655−665.

Biesiekierski, A., Wang, J., Gepreel, M.A.-H., Wen, C., 2012. A new look at biomedical Ti-based shape memory alloys. Acta Biomater. 8, 1661−1669.

Blacker, T.D., Robbins, J., Owen, S.J., Aguilovalentin, M.A., Clark, B.W., Voth, T.E., 2015. PLATO platinum topology optimization. In: Sandia National Lab. SNL-NM), Albuquerque, NM (United States).

Bobbert, F.S.L., Zadpoor, A.A., 2017. Effects of bone substitute architecture and surface properties on cell response, angiogenesis, and structure of new bone. J. Mater. Chem. B 5, 6175−6192.

Bobbert, F.S.L., Lietaert, K., Eftekhari, A.A., Pouran, B., Ahmadi, S.M., Weinans, H., Zadpoor, A.A., 2017. Additively manufactured metallic porous biomaterials based on minimal surfaces: a unique combination of topological, mechanical, and mass transport properties. Acta Biomater. 53, 572−584.

Bormann, T., Müller, B., Schinhammer, M., Kessler, A., Peter, T., de Wild, M., 2014. Microstructure of selective laser melted nickel−titanium. Mater. Char. 94, 189−202.

Bose, S., Vahabzadeh, S., Bandyopadhyay, A., 2013. Bone tissue engineering using 3D printing. Mater. Today 16, 496−504.

Bourell, D., Kruth, J.P., Ming, L., Levy, G., Rosen, D., Beese, A.M., Adam, C., 2017. Materials for additive manufacturing. CIRP Ann. 66, 659−681.

Brajlih, T., Valentan, B., Balic, J., Drstvensek, I., 2011. Speed and accuracy evaluation of additive manufacturing machines. Rapid Prototyp. J. 17 (1), 64−75.

Brandl, E., Greitemeier, D., 2012. Microstructure of additive layer manufactured Ti−6Al−4V after exceptional post heat treatments. Mater. Lett. 81, 84−87.

Bucklen, B.S., Wettergreen, W.A., Yuksel, E., Liebschner, M.A.K., 2008. Bone-derived CAD library for assembly of scaffolds in computer-aided tissue engineering. Virtual Phys. Prototyp. 3, 13−23.

Buehler, W.J., Gilfrich, J.V., Wiley, R.C., 1963. Effect of low-temperature phase changes on the mechanical properties of alloys near composition TiNi. J. Appl. Phys. 34, 1475−1477.

Burton, H.E., Eisenstein, N.M., Lawless, B.M., Jamshidi, P., Segarra, M.A., Owen, A., Shepherd, D.E.T., Attallah, M.M., Grover, L.M., Cox, S.C., 2019. The design of additively manufactured lattices to increase the functionality of medical implants. Mater. Sci. Eng. C 94, 901−908.

Calignano, F., 2014. Design optimization of supports for overhanging structures in aluminum and titanium alloys by selective laser melting. Mater. Des. 64, 203−213.

Callens, S.J.P., Uyttendaele, R.J.C., Fratila-Apachitei, L.E., Zadpoor, A.A., 2020. Substrate curvature as a cue to guide spatiotemporal cell and tissue organization. Biomaterials 232, 119739.

Campoli, G., Borleffs, M.S., Yavari, S.A., Wauthle, R., Weinans, H., Zadpoor, A.A., 2013. Mechanical properties of open-cell metallic biomaterials manufactured using additive manufacturing. Mater. Des. 49, 957−965.

Carter, D.R., Spengler, D.M., 1978. Mechanical properties and composition of cortical bone. Clin. Orthop. Relat. Res. (1976−2007) 135, 192−217.

Challis, V.J., Roberts, A.P., Grotowski, J.F., Zhang, L.-C., Sercombe, T.B., 2010. Prototypes for bone implant scaffolds designed via topology optimization and manufactured by solid freeform fabrication. Adv. Eng. Mater. 12, 1106−1110.

Cho, H.-H., Cho, Y., Han, H.N., 2015. Finite element analysis for mechanical response of Ti foams with regular structure obtained by selective laser melting. Acta Mater. 97, 199−206.

Choy, S.Y., Sun, C.-N., Leong, K.F., Wei, J., 2017. Compressive properties of functionally graded lattice structures manufactured by selective laser melting. Mater. Des. 131, 112−120.

Chuah, H.G., Abd Rahim, I., Imran Yusof, M., 2010. Topology optimisation of spinal interbody cage for reducing stress shielding effect. Comput. Methods Biomech. Biomed. Eng. 13, 319−326.

Cosma, C., Kessler, J., Gebhardt, A., Campbell, I., Balc, N., 2020. Improving the mechanical strength of dental applications and lattice structures SLM processed. Materials 13, 905.

Croes, M., Bakhshandeh, S., van Hengel, I.A.J., Lietaert, K., van Kessel, K.P.M., Pouran, B., van der Wal, B.C.H., Vogely, H.C., Van Hecke, W., Fluit, A.C., 2018. Antibacterial and immunogenic behavior of silver coatings on additively manufactured porous titanium. Acta Biomater. 81, 315−327.

Cutolo, A., Neirinck, B., Lietaert, K., de Formanoir, C., Van Hooreweder, B., 2018. Influence of layer thickness and post-process treatments on the fatigue properties of CoCr scaffolds produced by laser powder bed fusion. Addit. Manuf. 23, 498−504.

Dallago, M., Fontanari, V., Torresani, E., Leoni, M., Pederzolli, C., Potrich, C., Benedetti, M., 2018. Fatigue and biological properties of Ti-6Al-4V ELI cellular structures with variously arranged cubic cells made by selective laser melting. J. Mech. Behav. Biomed. Mater. 78, 381−394.

Dallago, M., Winiarski, B., Zanini, F., Carmignato, S., Benedetti, M., 2019. On the effect of geometrical imperfections and defects on the fatigue strength of cellular lattice structures additively manufactured via selective laser melting. Int. J. Fatig. 124, 348−360.

Davidson, J.A., Mishra, A.K., Kovacs, P., Poggie, R.A., 1994. New surface-hardened, low-modulus, corrosion-resistant Ti-13Nb-13Zr alloy for total hip arthroplasty. Bio Med. Mater. Eng. 4, 231−243.

de Jonge, C.P., Kolken, H., Zadpoor, A.A., 2019. Non-auxetic mechanical metamaterials. Materials 12, 635.

de Krijger, J., Rans, C., Van Hooreweder, B., Lietaert, K., Pouran, B., Zadpoor, A.A., 2017. Effects of applied stress ratio on the fatigue behavior of additively manufactured porous biomaterials under compressive loading. J. Mech. Behav. Biomed. Mater. 70, 7−16.

Dérand III, P., Rännar, L.-E., Hirsch, J.-M., 2012. Imaging, virtual planning, design, and production of patient-specific implants and clinical validation in craniomaxillofacial surgery. Craniomaxillofacial Trauma Reconstr. 5, 137−143.

Deshpande, V.S., Fleck, N.A., Ashby, M.F., 2001a. Effective properties of the octet-truss lattice material. J. Mech. Phys. Solid. 49, 1747−1769.

Deshpande, V.S., Ashby, M.F., Fleck, N.A., 2001b. Foam topology: bending versus stretching dominated architectures. Acta Mater. 49, 1035−1040.

Ding, M., Lin, X., Liu, W., 2018. Three-dimensional morphometric properties of rod-and plate-like trabeculae in adolescent cancellous bone. J. Orthop. Trans. 12, 26−35.

Doube, M., Kłosowski, M.M., Arganda-Carreras, I., Cordelières, F.P., Dougherty, R.P., Jackson, J.S., Schmid, B., Hutchinson, J.R., Shefelbine, S.J., 2010. BoneJ: free and extensible bone image analysis in ImageJ. Bone 47, 1076−1079.

Du Plessis, A., Yadroitsava, I., Le Roux, S.G., Yadroitsev, I., Fieres, J., Reinhart, C., Rossouw, P., 2017. Prediction of mechanical performance of Ti6Al4V cast alloy based on microCT-based load simulation. J. Alloys Compd. 724, 267−274.

Du Plessis, A., Yadroitsava, I., Yadroitsev, I., le Roux, S.G., Blaine, D.C., 2018a. Numerical comparison of lattice unit cell designs for medical implants by additive manufacturing. Virtual Phys. Prototyp. 13, 266−281.

Du Plessis, A., Kouprianoff, D.-P., Yadroitsava, I., Yadroitsev, I., 2018b. Mechanical properties and in situ deformation imaging of microlattices manufactured by laser based powder bed fusion. Materials 11, 1663.

Du Plessis, A., Razavi, S.M.J., Berto, F., 2020. The effects of microporosity in struts of gyroid lattice structures produced by laser powder bed fusion. Mater. Des. 194, 108899.

El Elmi, A., Melancon, D., Asgari, M., Liu, L., Pasini, D., 2020. Experimental and numerical investigation of selective laser melting−induced defects in Ti−6Al−4V octet truss lattice material: the role of material microstructure and morphological variations. J. Mater. Res. 35, 1900−1912.

Elahinia, M.H., Hashemi, M., Tabesh, M., Bhaduri, S.B., 2012. Manufacturing and processing of NiTi implants: a review. Prog. Mater. Sci. 57, 911−946.

Erbel, R., Di Mario, C., Bartunek, J., Bonnier, J., de Bruyne, B., Eberli, F.R., Paul, E., Haude, M., Heublein, B., Horrigan, M., 2007. Temporary scaffolding of coronary arteries with bioabsorbable magnesium stents: a prospective, non-randomised multicentre trial. Lancet 369, 1869−1875.

Fischer, M., Joguet, D., Robin, G., Peltier, L., Laheurte, P., 2016. In situ elaboration of a binary Ti−26Nb alloy by selective laser melting of elemental titanium and niobium mixed powders. Mater. Sci. Eng. C 62, 852−859.

Fraldi, M., Esposito, L., Perrella, G., Cutolo, A., Cowin, S.C., 2010. Topological optimization in hip prosthesis design. Biomech. Model. Mechanobiol. 9, 389−402.

Frazier, W.E., 2014. Metal additive manufacturing: a review. J. Mater. Eng. Perform. 23, 1917−1928.

Ganjian, M., Angeloni, L., Mirzaali, M.J., Modaresifar, K., Hagen, C.W., Ghatkesar, M.K., Leon Hagedoorn, P., Fratila-Apachitei, L., Zadpoor, A.A., 2020. Quantitative mechanics of 3D printed nanopillars interacting with bacterial cells. Nanoscale 12, 21988−22001. https://doi.org/10.1039/D0NR05984F (Communication).

Garner, E., Kolken, H.M.A., Wang, C.C.L., Zadpoor, A.A., Wu, J., 2019. Compatibility in microstructural optimization for additive manufacturing. Addit. Manuf. 26, 65−75.

Gatt, R., Wood, M.V., Gatt, A., Zarb, F., Formosa, C., Azzopardi, K.M., Casha, A., Agius, T.P., Schembri-Wismayer, P., Attard, L., 2015. Negative poisson's ratios in tendons: an unexpected mechanical response. Acta Biomater. 24, 201−208.

Ge, J., Huang, J., Lei, Y., O'Reilly, P., Ahmed, M., Zhang, C., Yan, X., Yin, S., 2020. Microstructural features and compressive properties of SLM Ti6Al4V lattice structures. Surf. Coat. Technol. 403, 126419.

Geng, H., Poologasundarampillai, G., Todd, N., Devlin-Mullin, A., Moore, K.L., Golrokhi, Z., Gilchrist, J.B., Jones, E., Potter, R.J., Sutcliffe, C., 2017. Biotransformation of silver released from nanoparticle coated titanium implants revealed in regenerating bone. ACS Appl. Mater. Interfaces 9, 21169−21180.

Genovese, K., Sander, L., Zadpoor, A.A., 2017. Microscopic full-field three-dimensional strain measurement during the mechanical testing of additively manufactured porous biomaterials. J. Mech. Behav. Biomed. Mater. 69, 327−341.

Gepreel, M.A.-H., Niinomi, M., 2013. Biocompatibility of Ti-alloys for long-term implantation. J. Mech. Behav. Biomed. Mater. 20, 407−415.

Ghouse, S., Babu, S., Van Arkel, R.J., Nai, K., Hooper, P.A., Jeffers, J.R.T., 2017. The influence of laser parameters and scanning strategies on the mechanical properties of a stochastic porous material. Mater. Des. 131, 498−508.

Giannitelli, S.M., Accoto, D., Trombetta, M., Rainer, A., 2014. Current trends in the design of scaffolds for computer-aided tissue engineering. Acta Biomater. 10, 580−594.

Gibson, L.J., Ashby, M.F., 1999. Cellular Solids: Structure and Properties. Cambridge University Press.

Gibson, I., Rosen, D.W., Stucker, B., 2014. Additive Manufacturing Technologies. Springer.

Gockel, J., Beuth, J., 2013. Understanding Ti-6Al-4V microstructure control in additive manufacturing via process maps. In: Solid Freeform Fabrication Proceedings. University of Texas, Austin, pp. 666−674.

Gokuldoss, P.K., Kolla, S., Eckert, J., 2017. Additive manufacturing processes: selective laser melting, electron beam melting and binder jetting—selection guidelines. Materials 10, 672.

Goldstein, S.A., 1987. The mechanical properties of trabecular bone: dependence on anatomic location and function. J Biomech 20 (11−12), 1055−1061.

Gorgin Karaji, Z., Speirs, M., Dadbakhsh, S., Kruth, J.-P., Weinans, H., Zadpoor, A.A., Amin Yavari, S., 2017. Additively manufactured and surface biofunctionalized porous nitinol. ACS Appl. Mater. Interfaces 9, 1293−1304.

Großmann, A., Gosmann, J., Mittelstedt, C., 2019. Lightweight lattice structures in selective laser melting: design, fabrication and mechanical properties. Mater. Sci. Eng. A 766, 138356.

Gu, D., Shen, Y., 2009. Balling phenomena in direct laser sintering of stainless steel powder: metallurgical mechanisms and control methods. Mater. Des. 30, 2903−2910.

Guest, J.K., Prévost, J.H., 2006. Optimizing multifunctional materials: design of microstructures for maximized stiffness and fluid permeability. Int. J. Solid Struct. 43, 7028−7047.

Haberland, C., Elahinia, M., Walker, J.M., Meier, H., Frenzel, J., 2014. On the development of high quality NiTi shape memory and pseudoelastic parts by additive manufacturing. Smart Mater. Struct. 23, 104002.

Habijan, T., Haberland, C., Meier, H., Frenzel, J., Wittsiepe, J., Wuwer, C., Greulich, C., Schildhauer, T.A., Köller, M., 2013. The biocompatibility of dense and porous nickel−titanium produced by selective laser melting. Mater. Sci. Eng. C 33, 419−426.

Han, C., Li, Y., Wang, Q., Wen, S., Wei, Q., Yan, C., Liang, H., Liu, J., Shi, Y., 2018. Continuous functionally graded porous titanium scaffolds manufactured by selective laser melting for bone implants. J. Mech. Behav. Biomed. Mater. 80, 119−127.

Han, Q., Gu, Y., Setchi, R., Lacan, F., Johnston, R., Evans, S.L., Yang, S., 2019. Additive manufacturing of high-strength crack-free Ni-based hastelloy X superalloy. Addit. Manuf. 30, 100919.

Hashin, Z., Shtrikman, S., 1963. A variational approach to the theory of the elastic behaviour of multiphase materials. J. Mech. Phys. Solid. 11, 127−140.

Hedayati, R., Hosseini-Toudeshky, H., Sadighi, M., Mohammadi-Aghdam, M., Zadpoor, A.A., 2016a. Computational prediction of the fatigue behavior of additively manufactured porous metallic biomaterials. Int. J. Fatig. 84, 67−79.

Hedayati, R., Sadighi, M., Mohammadi-Aghdam, M., Zadpoor, A.A., 2016b. Effect of mass multiple counting on the elastic properties of open-cell regular porous biomaterials. Mater. Des. 89, 9−20.

Hedayati, R., Sadighi, M., Mohammadi-Aghdam, M., Zadpoor, A.A., 2016c. Mechanical properties of regular porous biomaterials made from truncated cube repeating unit cells: analytical solutions and computational models. Mater. Sci. Eng. C 60, 163−183.

Hedayati, R., Sadighi, M., Mohammadi-Aghdam, M., Zadpoor, A.A., 2016d. Mechanics of additively manufactured porous biomaterials based on the rhombicuboctahedron unit cell. J. Mech. Behav. Biomed. Mater. 53, 272−294.

Hedayati, R., Sadighi, M., Mohammadi-Aghdam, M., Zadpoor, A.A., 2017. Analytical relationships for the mechanical properties of additively manufactured porous biomaterials based on octahedral unit cells. Appl. Math. Model. 46, 408−422.

Hedayati, R., Ahmadi, S.M., Lietaert, K., Pouran, B., Li, Y., Weinans, H., Rans, C.D., Zadpoor, A.A., 2018a. Isolated and modulated effects of topology and material type on the mechanical properties of additively manufactured porous biomaterials. J. Mech. Behav. Biomed. Mater. 79, 254−263.

Hedayati, R., Hosseini-Toudeshky, H., Sadighi, M., Mohammadi-Aghdam, M., Zadpoor, A.A., 2018b. Multiscale modeling of fatigue crack propagation in additively manufactured porous biomaterials. Int. J. Fatig. 113, 416−427.

Hedayati, R., Mirzaali, M.J., Vergani, L., Zadpoor, A.A., 2018c. Action-at-a-distance metamaterials: distributed local actuation through far-field global forces. APL Mater. 6, 036101.

Hoffmann, W., Bormann, T., Rossi, A., Müller, B., Schumacher, R., Martin, I., de Wild, M., Wendt, D., 2014. Rapid prototyped porous nickel−titanium scaffolds as bone substitutes. J. Tissue Eng. 5, 2041731414540674.

Hollister, S.J., Levy, R.A., Chu, T.-M., Halloran, J.W., Feinberg, S.E., 2000. An image-based approach for designing and manufacturing craniofacial scaffolds. Int. J. Oral Maxillofac. Surg. 29, 67−71.

Hollister, S.J., Maddox, R.D., Taboas, J.M., 2002. Optimal design and fabrication of scaffolds to mimic tissue properties and satisfy biological constraints. Biomaterials 23, 4095−4103.

Hou, Y., Jia, G., Yue, R., Chen, C., Jia, P., Zhang, H., Huang, H., Xiong, M., Yuan, G., 2018. Synthesis of biodegradable Zn-based scaffolds using NaCl templates: relationship between porosity, compressive properties and degradation behavior. Mater. Char. 137, 162−169.

Huang, X., Xie, Y.M., 2007. Bidirectional evolutionary topology optimization for structures with geometrical and material nonlinearities. AIAA J. 45, 308−313.

Huang, X., Xie, Y.M., 2009. Bi-directional evolutionary topology optimization of continuum structures with one or multiple materials. Comput. Mech. 43, 393.

Huang, X., Lang, L., Gong, S., Zhao, M., 2020. Effect of post-treatment on the microstructure and mechanical properties of selective laser melted Ti6Al4V lattice structures. Rapid Prototyp. J. 26.

Hussein, A., Liang, H., Yan, C., Everson, R., Young, P., 2013. Advanced lattice support structures for metal additive manufacturing. J. Mater. Process. Technol. 213, 1019−1026.

Janbaz, S., Hedayati, R., Zadpoor, A.A., 2016. Programming the shape-shifting of flat soft matter: from self-rolling/self-twisting materials to self-folding origami. Mater. Horiz. 3, 536−547.

Janbaz, S., Bobbert, F.S.L., Mirzaali, M.J., Zadpoor, A.A., 2019. Ultra-programmable buckling-driven soft cellular mechanisms. Mater. Horiz. 6, 1138−1147.

Janbaz, S., Narooei, K., van Manen, T., Zadpoor, A.A., 2020. Strain rate−dependent mechanical metamaterials. Sci. Adv. 6, eaba0616.

Jardini, A.L., Aparecida Larosa, M., Maciel Filho, R., de Carvalho Zavaglia, C.A., Bernardes, L.F., Lambert, C.S., Reis Calderoni, D., Kharmandayan, P., 2014. Cranial reconstruction: 3D biomodel and custom-built implant created using additive manufacturing. J. Cranio-Maxillofacial Surg. 42, 1877−1884.

Juillet, C., Oudriss, A., Balmain, J., Feaugas, X., Pedraza, F., 2018. Characterization and oxidation resistance of additive manufactured and forged IN718 Ni-based superalloys. Corrosion Sci. 142, 266−276.

Kadkhodapour, J., Montazerian, H., Darabi, A.C., Anaraki, A.P., Ahmadi, S.M., Zadpoor, A.A., Schmauder, S., 2015. Failure mechanisms of additively manufactured porous biomaterials: effects of porosity and type of unit cell. J. Mech. Behav. Biomed. Mater. 50, 180−191.

Kajima, Y., Takaichi, A., Nakamoto, T., Kimura, T., Yogo, Y., Ashida, M., Doi, H., Nomura, N., Takahashi, H., Takao, H., 2016. Fatigue strength of Co−Cr−Mo alloy clasps prepared by selective laser melting. J. Mech. Behav. Biomed. Mater. 59, 446−458.

Kapfer, S.C., Hyde, S.T., Mecke, K., Arns, C.H., Schröder-Turk, G.E., 2011. Minimal surface scaffold designs for tissue engineering. Biomaterials 32, 6875−6882.

Karageorgiou, V., Kaplan, D., 2005. Porosity of 3D biomaterial scaffolds and osteogenesis. Biomaterials 26, 5474−5491.

Karaji, Z.G., Hedayati, R., Pouran, B., Apachitei, I., Zadpoor, A.A., 2017. Effects of plasma electrolytic oxidation process on the mechanical properties of additively manufactured porous biomaterials. Mater. Sci. Eng. C 76, 406−416.

Kataria, R., Singh, R.P., Sharma, P., Phanden, R.K., 2020. Welding of super alloys: a review. Mater. Today Proc. https://doi.org/10.1016/j.matpr.2020.07.198.

Katarivas Levy, G., Goldman, J., Aghion, E., 2017. The prospects of zinc as a structural material for biodegradable implants—a review paper. Metals 7, 402.

Kelly, C.N., Francovich, J., Julmi, S., Safranski, D., Guldberg, R.E., Maier, H.J., Gall, K., 2019. Fatigue behavior of as-built selective laser melted titanium scaffolds with sheet-based gyroid microarchitecture for bone tissue engineering. Acta Biomater. 94, 610−626.

Kok, Y., Tan, X.P., Wang, P., Nai, M.L.S., Loh, N.H., Liu, E., Tor, S.B., 2018. Anisotropy and heterogeneity of microstructure and mechanical properties in metal additive manufacturing: a critical review. Mater. Des. 139, 565−586.

Kolken, H.M.A., Zadpoor, A.A., 2017. Auxetic mechanical metamaterials. RSC Adv. 7, 5111−5129.

Kolken, H.M.A., Janbaz, S., Leeflang, S.M.A., Lietaert, K., Weinans, H.H., Zadpoor, A.A., 2018. Rationally designed meta-implants: a combination of auxetic and conventional meta-biomaterials. Mater. Horiz. 5, 28−35.

Köster, R., Vieluf, D., Kiehn, M., Sommerauer, M., Jan, K., Baldus, S., Meinertz, T., Hamm, C.W., 2000. Nickel and molybdenum contact allergies in patients with coronary in-stent restenosis. Lancet 356, 1895−1897.

Krakhmalev, P., Yadroitsev, I., Yadroitsava, I., De Smidt, O., 2017. Functionalization of biomedical Ti6Al4V via in situ alloying by cu during laser powder bed fusion manufacturing. Materials 10, 1154.

Kranz, J., Herzog, D., Emmelmann, C., 2015. Design guidelines for laser additive manufacturing of lightweight structures in TiAl6V4. J. Laser Appl. 27, S14001.

Krol, T.A., Zaeh, M.F., Seidel, C., 2012. Optimization of Supports in Metal-Based Additive Manufacturing by Means of Finite Element Models. Bourell DL.

Kuroda, D., Niinomi, M., Morinaga, M., Kato, Y., Yashiro, T., 1998. Design and mechanical properties of new β type titanium alloys for implant materials. Mater. Sci. Eng. A 243, 244−249.

Langelaar, M., 2018. Combined optimization of part topology, support structure layout and build orientation for additive manufacturing. Struct. Multidiscip. Optim. 57, 1985−2004.

Leary, M., Mazur, M., Williams, H., Yang, E., Ahmad, A., Lozanovski, B., Zhang, X., Shidid, D., Farahbod-Sternahl, L., Witt, G., 2018. Inconel 625 lattice structures manufactured by selective laser melting (SLM): mechanical properties, deformation and failure modes. Mater. Des. 157, 179−199.

Li, H., Zheng, Y., Qin, L., 2014a. Progress of biodegradable metals. Prog. Nat. Sci. Mater. Int. 24, 414−422.

Li, S.J., Xu, Q.S., Wang, Z., Hou, W.T., Hao, Y.L., Yang, R., Murr, L.E., 2014b. Influence of cell shape on mechanical properties of Ti−6Al−4V meshes fabricated by electron beam melting method. Acta Biomater. 10, 4537−4547.

Li, W., Zhou, J., Xu, Y., 2015. Study of the in vitro cytotoxicity testing of medical devices. Biomed. Rep. 3, 617−620.

Li, S., Xiao, H., Liu, K., Xiao, W., Li, Y., Han, X., Mazumder, J., Song, L., 2017. Melt-pool motion, temperature variation and dendritic morphology of inconel 718 during pulsed- and continuous-wave laser additive manufacturing: a comparative study. Mater. Des. 119, 351−360.

Li, Y., Jahr, H., Lietaert, K., Pavanram, P., Yilmaz, A., Fockaert, L.I., Leeflang, M.A., Pouran, B., Gonzalez-Garcia, Y., Weinans, H., 2018a. Additively manufactured biode-gradable porous iron. Acta Biomater. 77, 380−393.

Li, Y., Zhou, J., Pavanram, P., MA, L., LI, F., Pouran, B., Tümer, N., Schröder, K.-U., Mol, J.M.C., Weinans, H., 2018b. Additively manufactured biodegradable porous mag-nesium. Acta Biomater. 67, 378−392.

Li, Y., Pavanram, P., Zhou, J., Lietaert, K., Taheri, P., Li, W., San, H., Leeflang, M.A., Mol, J.M.C., Jahr, H., 2020a. Additively manufactured biodegradable porous zinc. Acta Biomater. 101, 609−623.

Li, Y., Jahr, H., Zhou, J., Zadpoor, A.A., 2020b. Additively manufactured biodegradable porous metals. Acta Biomater. 115, 29−50.

Liang, S.-X., Wang, X., Zhang, W., Liu, Y.-J., Wang, W., Zhang, L.-C., 2020. Selective laser melting manufactured porous Fe-based metallic glass matrix composite with remarkable catalytic activity and reusability. Appl. Mater. Today 19, 100543.

Lietaert, K., Cutolo, A., Boey, D., Van Hooreweder, B., 2018. Fatigue life of additively manufactured Ti6Al4V scaffolds under tension-tension, tension-compression and compression-compression fatigue load. Sci. Rep. 8, 1−9.

Lin, C.-Y., Wirtz, T., Frank, L.M., Hollister, S.J., 2007. Structural and mechanical evaluations of a topology optimized titanium interbody fusion cage fabricated by selective laser melting process. J. Biomed. Mater. Res. A 83, 272−279.

Liu, Y.J., Wang, H.L., Li, S.J., Wang, S.G., Wang, W.J., Hou, W.T., Hao, Y.L., Yang, R., Zhang, L.C., 2017. Compressive and fatigue behavior of beta-type titanium porous structures fabricated by electron beam melting. Acta Mater. 126, 58−66.

Loh, G.H., Pei, E., Harrison, D., Monzon, M.D., 2018. An overview of functionally graded additive manufacturing. Addit. Manuf. 23, 34−44.

Long, M., Rack, H.J., 1998. Titanium alloys in total joint replacement—a materials science perspective. Biomaterials 19, 1621−1639.

Lozanovski, B., Downing, D., Tino, R., Du Plessis, A., Tran, P., Jakeman, J., Shidid, D., Emmelmann, C., Qian, M., Peter, C., 2020. Non-destructive simulation of node defects in additively manufactured lattice structures. Addit. Manuf. 36, 101593.

Łyczkowska, E., Szymczyk, P., Dybała, B., Chlebus, E., 2014. Chemical polishing of scaffolds made of Ti-6Al-7Nb alloy by additive manufacturing. Arch. Civil Mech. Eng. 14, 586−594.

Maconachie, T., Leary, M., Lozanovski, B., Zhang, X., Qian, M., Faruque, O., Brandt, M., 2019. SLM lattice structures: properties, performance, applications and challenges. Mater. Des. 183, 108137.

Maloney, K.J., Fink, K.D., Schaedler, T.A., Kolodziejska, J.A., Jacobsen, A.J., Roper, C.S., 2012. Multifunctional heat exchangers derived from three-dimensional micro-lattice structures. Int. J. Heat Mass Tran. 55, 2486−2493.

Mandal, A., Tiwari, J.K., AlMangour, B., Sathish, N., Kumar, S., Kamaraj, M., Ashiq, M., Srivastava, A.K., 2020. Tribological behavior of graphene-reinforced 316L stainless-steel composite prepared via selective laser melting. Tribol. Int. 151, 106525.

Maskery, I., Aboulkhair, N.T., Aremu, A.O., Tuck, C.J., Ashcroft, I.A., 2017. Compressive failure modes and energy absorption in additively manufactured double gyroid lattices. Addit. Manuf. 16, 24−29.

Mertens, C., Hubert, L., Hoffmann, J., 2013. Image data based reconstruction of the midface using a patient-specific implant in combination with a vascularized osteomyocutaneous scapular flap. J. Cranio-Maxillofacial Surg. 41, 219−225.

Mirzaali, M.J., Alexander, B., Schwiedrzik, J., Zysset, P.K., Wolfram, U., 2015. Continuum damage interactions between tension and compression in osteonal bone. J. Mech. Behav. Biomed. Mater. 49, 355−369.

Mirzaali, M.J., Libonati, F., Vena, P., Mussi, V., Vergani, L., Strano, M., 2016a. Investigation of the effect of internal pores distribution on the elastic properties of closed-cell aluminum foam: a comparison with cancellous bone. Procedia Struct. Integrity 2, 1285−1294.

Mirzaali, M.J., Schwiedrzik, J.J., Thaiwichai, S., Best, J.P., Michler, J., Zysset, P.K., Wolfram, U., 2016b. Mechanical properties of cortical bone and their relationships with age, gender, composition and microindentation properties in the elderly. Bone 93, 196−211.

Mirzaali, M.J., Habibi, M., Janbaz, S., Vergani, L., Zadpoor, A.A., 2017a. Crumpling-based soft metamaterials: the effects of sheet pore size and porosity. Sci. Rep. 7, 1−7.

Mirzaali, M.J., Hedayati, R., Vena, P., Vergani, L.A.U.R.A., Strano, M., Zadpoor, A.A., 2017b. Rational design of soft mechanical metamaterials: independent tailoring of elastic properties with randomness. Appl. Phys. Lett. 111, 051903.

Mirzaali, M.J., Mussi, V., Vena, P., Libonati, F., Vergani, L., Strano, M., 2017c. Mimicking the loading adaptation of bone microstructure with aluminum foams. Mater. Des. 126, 207−218.

Mirzaali, M.J., Janbaz, S., Strano, M., Vergani, L., Zadpoor, A.A., 2018a. Shape-matching soft mechanical metamaterials. Sci. Rep. 8, 1−7.

Mirzaali, M.J., Libonati, F., Ferrario, D., Rinaudo, L., Messina, C., Ulivieri, F.M., Cesana, B.M., Strano, M., Vergani, L., 2018b. Determinants of bone damage: an ex-vivo study on porcine vertebrae. PLoS One 13, e0202210.

Mirzaali, M.J., Bobbert, F.S.L., Li, Y., Zadpoor, A.A., 2019a. 4 additive manufacturing of metals using powder bed-based technologies. Addit. Manuf. 93.

Mirzaali, M.J., Libonati, F., Böhm, C., Rinaudo, L., Cesana, B.M., Ulivieri, F.M., Vergani, L., 2020. Fatigue-caused damage in trabecular bone from clinical, morphological and mechanical perspectives. Int. J. Fatig. 133, 105451.

Mitchell, A., Lafont, U., Hołyńska, M., Semprimoschnig, C.J.A.M., 2018. Additive manufacturing—a review of 4D printing and future applications. Addit. Manuf. 24, 606−626.

Miyazaki, S., Kim, H.Y., Hosoda, H., 2006. Development and characterization of Ni-free Ti-base shape memory and superelastic alloys. Mater. Sci. Eng. A 438, 18−24.

Miyoshi, T., Itoh, M., Akiyama, S., Kitahara, A., 2000. ALPORAS aluminum foam: production process, properties, and applications. Adv. Eng. Mater. 2, 179−183.

Mohammed, M.I., Gibson, I., 2018. Design of three-dimensional, triply periodic unit cell scaffold structures for additive manufacturing. J. Mech. Des. 140.

Mohammed, M., Fitzpatrick, A., Malyala, S., Gibson, I., 2016. Customised design and development of patient specific 3D printed whole mandible implant. In: Proceedings of the 27th Annual International Solid Freeform Fabrication Symposium, pp. 1708−1717.

Monzón, M., Liu, C., Ajami, S., Oliveira, M., Donate, R., Ribeiro, V., Reis, R.L., 2018. Functionally graded additive manufacturing to achieve functionality specifications of osteochondral scaffolds. Bio-Des. Manuf. 1, 69−75.

Morgan, N.B., 2004. Medical shape memory alloy applications—the market and its products. Mater. Sci. Eng. A 378, 16−23.

Murr, L.E., Gaytan, S.M., Medina, F., Lopez, H., Martinez, E., Machado, B.I., Hernandez, D.H., Martinez, L., Lopez, M.I., Wicker, R.B., 2010. Next-generation biomedical implants using additive manufacturing of complex, cellular and functional mesh arrays. Phil. Trans. R. Soc. A Math. Phys. Eng. Sci. 368, 1999−2032.

Nagesha, B.K., Dhinakaran, V., Varsha Shree, M., Manoj Kumar, K.P., Chalawadi, D., Sathish, T., 2020. Review on characterization and impacts of the lattice structure in additive manufacturing. Mater. Today Proc. 21, 916−919.

Nam, J., Starly, B., Darling, A., Sun, W., 2004. Computer aided tissue engineering for modeling and design of novel tissue scaffolds. Comput.-Aided Des. Appl. 1, 633−640.

Nickels, L., 2012. World's first patient-specific jaw implant. Met. Powder Rep. 67, 12−14.

Niinomi, M., 2003. Recent research and development in titanium alloys for biomedical applications and healthcare goods. Sci. Technol. Adv. Mater. 4, 445.

Niu, H.J., Chang, I.T.H., 1999. Instability of scan tracks of selective laser sintering of high speed steel powder. Scripta Mater. 41, 1229−1234.

Nouri-Goushki, M., Mirzaali, M.J., Angeloni, L., Fan, D., Minneboo, M., Ghatkesar, M.K., Staufer, U., Fratila-Apachitei, L.E., Zadpoor, A.A., 2019. 3D printing of large areas of highly ordered submicron patterns for modulating cell behavior. ACS Appl. Mater. Interfaces 12, 200−208.

Nune, K.C., Misra, R.D.K., Gai, X., Li, S.J., Hao, Y.L., 2018. Surface nanotopography-induced favorable modulation of bioactivity and osteoconductive potential of anodized 3D printed Ti-6Al-4V alloy mesh structure. J. Biomater. Appl. 32, 1032−1048.

Obbard, E.G., Hao, Y.L., Akahori, T., Talling, R.J., Niinomi, M., Dye, D., Yang, R., 2010. Mechanics of superelasticity in Ti−30Nb−(8−10) Ta−5Zr alloy. Acta Mater. 58, 3557−3567.

Parthasarathy, J., 2014. 3D modeling, custom implants and its future perspectives in craniofacial surgery. Ann. Maxillofacial Surg. 4, 9.

Putra, N.E., Mirzaali, M.J., Apachitei, I., Zhou, J., Zadpoor, A.A., 2020. Multi-material additive manufacturing technologies for Ti-, Mg-, and Fe-based biomaterials for bone substitution. Acta Biomater. 109, 1−20.

Rho, J.-Y., Kuhn-Spearing, L., Zioupos, P., 1998. Mechanical properties and the hierarchical structure of bone. Med. Eng. Phys. 20, 92−102.

Roy, S.C.D., 2014. Some recent work on lattice structures for digital signal processing. Sadhana 39, 1271−1294.

Ryan, G., Pandit, A., Apatsidis, D.P., 2006. Fabrication methods of porous metals for use in orthopaedic applications. Biomaterials 27, 2651−2670.

Salem, H., Carter, L.N., Attallah, M.M., Salem, H.G., 2019. Influence of processing parameters on internal porosity and types of defects formed in Ti6Al4V lattice structure fabricated by selective laser melting. Mater. Sci. Eng. A 767, 138387.

Sánchez-Palencia, E., 1980. Non-homogeneous media and vibration theory. Lect. Notes Phys. 127.

Sigmund, O., Torquato, S., 1997. Design of materials with extreme thermal expansion using a three-phase topology optimization method. J. Mech. Phys. Solid. 45, 1037−1067.

Sing, S.L., Wiria, F.E., Yeong, W.Y., 2018. Selective laser melting of lattice structures: a statistical approach to manufacturability and mechanical behavior. Robot. Comput. Integrated Manuf. 49, 170−180.

Song, B., Dong, S., Qi, L., Liao, H., Coddet, C., 2014. Vacuum heat treatment of iron parts produced by selective laser melting: microstructure, residual stress and tensile behavior. Mater. Des. (1980−2015) 54, 727−733.

Speirs, M., Van Hooreweder, B., Van Humbeeck, J., Kruth, J.-P., 2017. Fatigue behaviour of NiTi shape memory alloy scaffolds produced by SLM, a unit cell design comparison. J. Mech. Behav. Biomed. Mater. 70, 53−59.

Stevens, B., Yang, Y., Mohandas, A., Stucker, B., Nguyen, K.T., 2008. A review of materials, fabrication methods, and strategies used to enhance bone regeneration in engineered bone tissues. J. Biomed. Mater. Res. B 85, 573−582.

Strano, G., Liang, H., Everson, R.M., Evans, K.E., 2013. Surface roughness analysis, modelling and prediction in selective laser melting. J. Mater. Process. Technol. 213, 589−597.

Su, X.-bin, Yang, Y., Peng, Y.U., Sun, J.-feng, 2012. Development of porous medical implant scaffolds via laser additive manufacturing. Trans. Nonferrous Metals Soc. China 22, s181−s187.

Sun, Z.P., Guo, Y.B., Shim, V.P.W., 2020. Characterisation and modeling of additively-manufactured polymeric hybrid lattice structures for energy absorption. Int. J. Mech. Sci. 191, 106101.

Tammas-Williams, S., Withers, P.J., Todd, I., Prangnell, P.B., 2016. The effectiveness of hot isostatic pressing for closing porosity in titanium parts manufactured by selective electron beam melting. Metall. Mater. Trans. A 47, 1939−1946.

Tang, H.P., Qian, M., Liu, N., Zhang, X.Z., Yang, G.Y., Wang, J., 2015a. Effect of powder reuse times on additive manufacturing of Ti-6Al-4V by selective electron beam melting. J. Occup. Med. 67, 555−563.

Thöne, M., Leuders, S., Riemer, A., Tröster, T., HA, R., 2012. Influence of heat-treatment on selective laser melting products−eg Ti6Al4V. In: Solid Freeform Fabrication Symposium SFF, Austin Texas.

Van Bael, S., Chai, Y.C., Truscello, S., Moesen, M., Kerckhofs, G., Van Oosterwyck, H., Kruth, J.-P., Schrooten, J.J.A.B., 2012. The effect of pore geometry on the in vitro biological behavior of human periosteum-derived cells seeded on selective laser-melted Ti6Al4V bone scaffolds. Acta Biomater. 8, 2824−2834.

van der Stok, J., Wang, H., Yavari, S.A., Siebelt, M., Sandker, M., Waarsing, J.H., Verhaar, J.A.N., Jahr, H., Zadpoor, A.A., Leeuwenburgh, S.C.G., 2013. Enhanced bone regeneration of cortical segmental bone defects using porous titanium scaffolds incorporated with colloidal gelatin gels for time-and dose-controlled delivery of dual growth factors. Tissue Eng. A 19, 2605−2614.

van der Stok, J., Koolen, M.K.E., de Maat, M., Yavari, S.A., Alblas, J., Peter, P., Verhaar, J.A.N., van Lieshout, E., Zadpoor, A.A., Weinans, H., 2015a. Full regeneration of segmental bone defects using porous titanium implants loaded with BMP-2 containing fibrin gels. Eur. Cell. Mater. 141−154.

Van Der Stok, J., Lozano, D., Chai, Y.C., Yavari, S.A., Bastidas Coral, A.P., Verhaar, J.A.N., Gómez-Barrena, E., Jan, S., Jahr, H., Zadpoor, A.A., 2015b. Osteostatin-coated porous titanium can improve early bone regeneration of cortical bone defects in rats. Tissue Eng. A 21, 1495−1506.

Van Eijnatten, M., van Dijk, R., Dobbe, J., Streekstra, G., Koivisto, J., Wolff, J., 2018. CT image segmentation methods for bone used in medical additive manufacturing. Med. Eng. Phys. 51, 6−16.

van Hengel, I.A.J., Riool, M., Fratila-Apachitei, L.E., Witte-Bouma, J., Farrell, E., Zadpoor, A.A., Zaat, S.A.J., Apachitei, I., 2017. Selective laser melting porous metallic implants with immobilized silver nanoparticles kill and prevent biofilm formation by methicillin-resistant *Staphylococcus aureus*. Biomaterials 140, 1−15.

van Hengel, I.A.J., Tierolf, M.W.A.M., Valerio, V.P.M., Minneboo, M., Fluit, A.C., Fratila-Apachitei, L.E., Apachitei, I., Zadpoor, A.A., 2020. Self-defending additively manufactured bone implants bearing silver and copper nanoparticles. J. Mater. Chem. B 8, 1589−1602.

Van Hooreweder, B., Kruth, J.-P., 2017. Advanced fatigue analysis of metal lattice structures produced by selective laser melting. CIRP Ann. 66, 221−224.

Van Hooreweder, B., Apers, Y., Lietaert, K., Kruth, J.-P., 2017. Improving the fatigue performance of porous metallic biomaterials produced by selective laser melting. Acta Biomater. 47, 193−202.

Van Humbeeck, J., 2018. Additive manufacturing of shape memory alloys. Shape Mem. Superelasticity 4, 309−312.

van Manen, T., Janbaz, S., Zadpoor, A.A., 2018. Programming the shape-shifting of flat soft matter. Mater. Today 21, 144−163.

Vilardell, A.M., Takezawa, A., Du Plessis, A., Takata, N., Krakhmalev, P., Kobashi, M., Albu, M., Kothleitner, G., Yadroitsava, I., Yadroitsev, I., 2020. Mechanical behavior of in-situ alloyed Ti6Al4V (ELI)-3 at.% Cu lattice structures manufactured by laser powder bed fusion and designed for implant applications. J. Mech. Behav. Biomed. Mater. 104130.

Vilaro, T., Colin, C., Bartout, J.-D., 2011. As-fabricated and heat-treated microstructures of the Ti-6Al-4V alloy processed by selective laser melting. Metall. Mater. Trans. A 42, 3190−3199.

Vojtěch, D., Kubásek, J., Šerák, J., Novák, P., 2011. Mechanical and corrosion properties of newly developed biodegradable Zn-based alloys for bone fixation. Acta Biomater. 7, 3515−3522.

Vora, P., Mumtaz, K., Todd, I., Hopkinson, N., 2015. AlSi12 in-situ alloy formation and residual stress reduction using anchorless selective laser melting. Addit. Manuf. 7, 12−19.

Vrancken, B., Thijs, L., Kruth, J.-P., Van Humbeeck, J., 2012. Heat treatment of Ti6Al4V produced by selective laser melting: microstructure and mechanical properties. J. Alloys Compd. 541, 177−185.

Wang, M.Y., Wang, X., Guo, D., 2003. A level set method for structural topology optimization. Comput. Methods Appl. Mech. Eng. 192, 227−246.

Wang, Di, Yang, Y., Liu, R., Xiao, D., Sun, J., 2013. Study on the designing rules and processability of porous structure based on selective laser melting (SLM). J. Mater. Process. Technol. 213, 1734−1742.

Wang, X., Xu, S., Zhou, S., Xu, W., Leary, M., Peter, C., Qian, M., Brandt, M., Xie, Y.M., 2016. Topological design and additive manufacturing of porous metals for bone scaffolds and orthopaedic implants: a review. Biomaterials 83, 127−141.

Wang, Q., Han, C., Choma, T., Wei, Q., Yan, C., Song, B., Shi, Y., 2017a. Effect of Nb content on microstructure, property and in vitro apatite-forming capability of Ti-Nb alloys fabricated via selective laser melting. Mater. Des. 126, 268−277.

Wang, Z., Denlinger, E., Michaleris, P., Stoica, A.D., Dong, M., Beese, A.M., 2017b. Residual stress mapping in inconel 625 fabricated through additive manufacturing: method for neutron diffraction measurements to validate thermomechanical model predictions. Mater. Des. 113, 169−177.

Wang, X., Kustov, S., Van Humbeeck, J., 2018a. A short review on the microstructure, transformation behavior and functional properties of NiTi shape memory alloys fabricated by selective laser melting. Materials 11, 1683.

Wang, Y., Zhang, L., Daynes, S., Zhang, H., Feih, S., Wang, M.Y., 2018b. Design of graded lattice structure with optimized mesostructures for additive manufacturing. Mater. Des. 142, 114−123.

Wauthle, R., Ahmadi, S.M., Yavari, S.A., Mulier, M., Zadpoor, A.A., Weinans, H., Van Humbeeck, J., Kruth, J.-P., Schrooten, J., 2015a. Revival of pure titanium for dynamically loaded porous implants using additive manufacturing. Mater. Sci. Eng. C 54, 94−100.

Wauthle, R., Van Der Stok, J., Yavari, S.A., Van Humbeeck, J., Kruth, J.-P., Zadpoor, A.A., Weinans, H., Mulier, M., Schrooten, J., 2015b. Additively manufactured porous tantalum implants. Acta Biomater. 14, 217−225.

Wauthle, R., Vrancken, B., Beynaerts, B., Jorissen, K., Jan, S., Kruth, J.-P., Van Humbeeck, J., 2015c. Effects of build orientation and heat treatment on the microstructure and mechanical properties of selective laser melted Ti6Al4V lattice structures. Addit. Manuf. 5, 77−84.

Wen, P., Jauer, L., Voshage, M., Chen, Y., Poprawe, R., Schleifenbaum, J.H., 2018. Densification behavior of pure Zn metal parts produced by selective laser melting for manufacturing biodegradable implants. J. Mater. Process. Technol. 258, 128−137.

Windhagen, H., Radtke, K., Weizbauer, A., Diekmann, J., Noll, Y., Kreimeyer, U., Schavan, R., Stukenborg-Colsman, C., Waizy, H., 2013. Biodegradable magnesium-based screw clinically equivalent to titanium screw in hallux valgus surgery: short term results of the first prospective, randomized, controlled clinical pilot study. Biomed. Eng. Online 12, 62.

Wu, M.-W., Lai, P.-H., 2016. The positive effect of hot isostatic pressing on improving the anisotropies of bending and impact properties in selective laser melted Ti-6Al-4V alloy. Mater. Sci. Eng. A 658, 429−438.

Wu, J., Aage, N., Westermann, R., Sigmund, O., 2017a. Infill optimization for additive manufacturing—approaching bone-like porous structures. IEEE Trans. Visualization Comput. Graph. 24, 1127−1140.

Wu, M.-W., Chen, J.-K., Lin, B.-H., Chiang, P.-H., 2017b. Improved fatigue endurance ratio of additive manufactured Ti-6Al-4V lattice by hot isostatic pressing. Mater. Des. 134, 163−170.

Xiao, D., Yang, Y., Su, X., Wang, Di, Sun, J., 2013. An integrated approach of topology optimized design and selective laser melting process for titanium implants materials. Bio Med. Mater. Eng. 23, 433−445.

Xie, Y.M., Steven, G.P., 1993. A simple evolutionary procedure for structural optimization. Comput. Struct. 49, 885−896.

Xie, Y.M., Steven, G.P., 1997. Basic evolutionary structural optimization. In: Evolutionary Structural Optimization. Springer.

Yakout, M., Elbestawi, M.A., Veldhuis, S.C., 2019. Density and mechanical properties in selective laser melting of Invar 36 and stainless steel 316L. J. Mater. Process. Technol. 266, 397−420.

Yan, C., Liang, H., Ahmed, H., Young, P., Raymont, D., 2014. Advanced lightweight 316L stainless steel cellular lattice structures fabricated via selective laser melting. Mater. Des. 55, 533−541.

Yan, C., Liang, H., Ahmed, H., Young, P., 2015. Ti−6Al−4V triply periodic minimal surface structures for bone implants fabricated via selective laser melting. J. Mech. Behav. Biomed. Mater. 51, 61−73.

Yan, Y., Li, Y., Song, L., Zeng, C., 2017. Pluripotent stem cell expansion and neural differentiation in 3-D scaffolds of tunable Poisson's ratio. Acta Biomater. 49, 192−203.

Yánez, A., Cuadrado, A., Martel, O., Afonso, H., Monopoli, D., 2018. Gyroid porous titanium structures: a versatile solution to be used as scaffolds in bone defect reconstruction. Mater. Des. 140, 21−29.

Yang, L., Yan, C., Cao, W., Liu, Z., Song, B., Wen, S., Zhang, C., Shi, Y., Yang, S., 2019. Compression−compression fatigue behaviour of gyroid-type triply periodic minimal surface porous structures fabricated by selective laser melting. Acta Mater. 181, 49−66.

Yavari, S.A., Wauthlé, R., van der Stok, J., Riemslag, A.C., Janssen, M., Mulier, M., Kruth, J.-P., Jan, S., Weinans, H., Zadpoor, A.A., 2013. Fatigue behavior of porous biomaterials manufactured using selective laser melting. Mater. Sci. Eng. C 33, 4849−4858.

Yavari, S.A., Ahmadi, S.M., van der Stok, J., Wauthlé, R., Riemslag, A.C., Janssen, M., Jan, S., Weinans, H., Zadpoor, A.A., 2014a. Effects of bio-functionalizing surface treatments on the mechanical behavior of open porous titanium biomaterials. J. Mech. Behav. Biomed. Mater. 36, 109−119.

Yavari, S.A., Wauthlé, R., Böttger, A.J., Jan, S., Weinans, H., Zadpoor, A.A., 2014b. Crystal structure and nanotopographical features on the surface of heat-treated and anodized porous titanium biomaterials produced using selective laser melting. Appl. Surf. Sci. 290, 287−294.

Yavari, S.A., Ahmadi, S.M., Wauthle, R., Pouran, B., Schrooten, J., Weinans, H., Zadpoor, A.A., 2015. Relationship between unit cell type and porosity and the fatigue behavior of selective laser melted meta-biomaterials. J. Mech. Behav. Biomed. Mater. 43, 91−100.

Yavari, S.A., Croes, M., Akhavan, B., Jahanmard, F., Eigenhuis, C.C., Dadbakhsh, S., Vogely, H.C., Bilek, M.M., Fluit, A.C., CHE, B., 2020. Layer by layer coating for bio-functionalization of additively manufactured meta-biomaterials. Addit. Manuf. 32, 100991.

Yoo, D.J., 2011a. Porous scaffold design using the distance field and triply periodic minimal surface models. Biomaterials 32, 7741−7754.

Yoo, D.-J., 2011b. Computer-aided porous scaffold design for tissue engineering using triply periodic minimal surfaces. Int. J. Precis. Eng. Manuf. 12, 61−71.

Youssef, S., Maire, E., Gaertner, R., 2005. Finite element modelling of the actual structure of cellular materials determined by X-ray tomography. Acta Mater. 53, 719−730.

Yuan, L., Ding, S., Wen, C., 2019a. Additive manufacturing technology for porous metal implant applications and triple minimal surface structures: a review. Bioact. Mater. 4, 56−70.

Yuan, S., Chua, C.K., Zhou, K., 2019b. 3D-Printed mechanical metamaterials with high energy absorption. Adv. Mater. Technol. 4, 1800419.

Zadpoor, A.A., 2013. Open forward and inverse problems in theoretical modeling of bone tissue adaptation. J. Mech. Behav. Biomed. Mater. 27, 249−261.

Zadpoor, A.A., 2015. Bone tissue regeneration: the role of scaffold geometry. Biomater. Sci. 3, 231−245.

Zadpoor, A.A., 2016. Mechanical meta-materials. Mater. Horiz. 3, 371−381.

Zadpoor, A.A., 2017. Design for additive bio-manufacturing: from patient-specific medical devices to rationally designed meta-biomaterials. Int. J. Mol. Sci. 18, 1607.

Zadpoor, A.A., 2018. Frontiers of additively manufactured metallic materials. In: Multidisciplinary Digital. Publishing Institute.

Zadpoor, A.A., 2019. Additively manufactured porous metallic biomaterials. J. Mater. Chem. B 7, 4088−4117.

Zadpoor, A.A., 2020. Meta-biomaterials. Biomater. Sci. 8, 18−38.

Zadpoor, A.A., Hedayati, R., 2016. Analytical relationships for prediction of the mechanical properties of additively manufactured porous biomaterials. J. Biomed. Mater. Res. A 104, 3164−3174.

Zadpoor, A.A., Campoli, G., Weinans, H., 2013. Neural network prediction of load from the morphology of trabecular bone. Appl. Math. Model. 37, 5260−5276.

Zargarian, A., Esfahanian, M., Kadkhodapour, J., Ziaei-Rad, S., 2016. Numerical simulation of the fatigue behavior of additive manufactured titanium porous lattice structures. Mater. Sci. Eng. C 60, 339−347.

Zargarian, A., Esfahanian, M., Kadkhodapour, J., Ziaei-Rad, S., Zamani, D., 2019. On the fatigue behavior of additive manufactured lattice structures. Theor. Appl. Fract. Mech. 100, 225−232.

Zhang, L.-C., Attar, H., 2016. Selective laser melting of titanium alloys and titanium matrix composites for biomedical applications: a review. Adv. Eng. Mater. 18, 463−475.

Zhang, X.Z., Leary, M., Tang, H.P., Song, T., Qian, M., 2018. Selective electron beam manufactured Ti-6Al-4V lattice structures for orthopedic implant applications: current status and outstanding challenges. Curr. Opin. Solid State Mater. Sci. 22, 75−99.

Zhang, X., Yocom, C.J., Mao, B., Liao, Y., 2019. Microstructure evolution during selective laser melting of metallic materials: a review. J. Laser Appl. 31, 031201.

Zhao, S., Li, S.J., Hou, W.T., Hao, Y.L., Yang, R., Misra, R.D.K., 2016. The influence of cell morphology on the compressive fatigue behavior of Ti-6Al-4V meshes fabricated by electron beam melting. J. Mech. Behav. Biomed. Mater. 59, 251−264.

Zhao, S., Li, S.J., Wang, S.G., Hou, W.T., Li, Y., Zhang, L.C., Hao, Y.L., Yang, R., Misra, R.D.K., Murr, L.E., 2018. Compressive and fatigue behavior of functionally graded Ti-6Al-4V meshes fabricated by electron beam melting. Acta Mater. 150, 1−15.

Zhao, Z., Li, J., Bai, P., Qu, H., Liang, M., Liao, H., Wu, L., Huo, P., Liu, H., Zhang, J., 2019. Microstructure and mechanical properties of TiC-reinforced 316L stainless steel composites fabricated using selective laser melting. Metals 9, 267.

Zheng, Y.F., Gu, X.N., Witte, F., 2014. Biodegradable metals. Mater. Sci. Eng. R Rep. 77, 1−34.

Zhou, M., Rozvany, G.I.N., 1991. The COC algorithm, Part II: topological, geometrical and generalized shape optimization. Comput. Methods Appl. Mech. Eng. 89, 309−336.

Zhou, J., Shrotriya, P., Soboyejo, W.O., 2004. On the deformation of aluminum lattice block structures: from struts to structures. Mech. Mater. 36, 723−737.

Zhou, J., Dong, J., Wang, B., Koschny, T., Kafesaki, M., Soukoulis, C.M., 2009. Negative refractive index due to chirality. Phys. Rev. B 79, 121104.